Azimuthal Shear of a Transversely Isotropic Elastic Solid

F. KASSIANIDIS
R. W. OGDEN
Department of Mathematics, University of Glasgow, University Gardens, Glasgow G12 8QW, UK

J. MERODIO
Department of Continuum Mechanics and Structures, E.T.S. Ingenieros Caminos, Canales y Puertos, Universidad Politecnica de Madrid, 28040, Madrid, Spain

T. J. PENCE
Department of Mechanical Engineering, Michigan State University, East Lansing, MI 48824, USA

Abstract: In this paper we study the problem of (plane strain) azimuthal shear of a circular cylindrical tube of incompressible *transversely isotropic* elastic material subject to finite deformation. The preferred direction associated with the transverse isotropy lies in the planes normal to the tube axis and is at an angle with the radial direction that depends only on the radius. For a general form of strain-energy function the considered deformation yields simple expressions for the azimuthal shear stress and the associated strong ellipticity condition in terms of the azimuthal shear strain. These apply for a sense of shear that is either "with" or "against" the preferred direction (anticlockwise and clockwise, respectively), so that material line elements locally in the preferred direction either extend or (at least initially) contract, respectively. For some specific strain-energy functions we then examine local loss of uniqueness of the shear stress-strain relationship and failure of ellipticity for the case of contraction and the dependence on the geometry of the preferred direction. In particular, for a reinforced neo-Hookean material, we obtain closed-form solutions that determine the domain of strong ellipticity in terms of the relationship between the shear strain and the angle (in general, a function of the radius) between the tangent to the preferred direction and the undeformed radial direction. It is shown, in particular, that as the magnitude of the applied shear stress increases then, after loss of ellipticity, there are two admissible values for the shear strain at certain radial locations. Absolutely stable deformations involve the lower magnitude value outside a certain radius and the higher magnitude value within this radius. The radius that separates the two values increases with increasing magnitude of the shear stress. The results are illustrated graphically for two specific forms of energy function.

Key Words: Large deformations, finite elasticity, transverse isotropy, azimuthal shear, loss of ellipticity

1. INTRODUCTION

The problem of azimuthal shear of a circular cylindrical tube composed of elastic material has been discussed in many publications since the pioneering work of Rivlin , primarily for *isotropic* elastic solids, compressible or incompressible. A review of the literature is provided by Jiang and Ogden , to which reference can be made for detailed citations. To the best of our knowledge, relatively little has been done for *anisotropic* bodies undergoing azimuthal shear deformation, although Jiang and Beatty examined the helical shear problem (of which the azimuthal shear problem is a special case) for transversely elastic materials whose direction of transverse isotropy is either axial, circumferential or helical; also, for transversely isotropic materials, Tsai and Fan analyzed the anti-plane shear problem. In both cases the attention of these authors was focussed mainly on constructing classes of strain-energy functions capable of undergoing the considered deformations. See also the recent contribution by Merodio concerned with the rectilinear shear of a slab of fiber-reinforced elastic material.

In the work of Abeyaratne the azimuthal shear problem has been studied in detail for incompressible, isotropic elastic materials from the point of view of loss of ellipticity. Specifically, loss of ellipticity, at intermediate ranges of loading applied at the boundaries of the tube heralds the emergence of certain non-smooth solutions. The existence of such solutions requires that the strain energy be non-convex as a function of the shear strain. In the present paper we examine the problem of azimuthal shear for a circular cylindrical tube of *transversely isotropic* elastic material in terms of loss of ellipticity, which requires loss of strict convexity of the strain energy as a function of the shear strain. The direction of transverse isotropy (the preferred direction) is taken to lie in planes normal to the axis of the tube so that the problem has a plane strain character. Moreover, this direction depends (in general) only on the radius through the material so that circular symmetry is maintained.

In Section 2, the geometry of the problem and the kinematics associated with the azimuthal shear deformation are introduced, while the form of the strain-energy function for a transversely isotropic material with the restriction to plane strain is given together with the (in-plane) Cauchy stress tensor and its polar components in Section 3. The components of the equilibrium equation are then summarized in Section 4. In Section 5 the form of the strong ellipticity condition appropriate for the considered specialization is stated. We consider a special class of material models consisting of an isotropic base material augmented by a reinforcement dependent on the preferred direction. As is known from the isotropic problem [6], loss of ellipticity requires loss of monotonicity of the shear stress versus shear strain relationship; in other words, a strain energy that is a non-convex function of the amount of shear. This is also the case here although the chosen energy function is non-convex only for negative shear strain.

The well-known neo-Hookean model augmented with the so-called *standard reinforcing model* is then the focus of attention in Section 6. The notion of strong ellipticity is studied in terms of the magnitude and direction of the applied (azimuthal shear) loading and the resulting shear strain in the material. Closed-form solutions are derived that determine the domain of strong ellipticity, on the boundaries of which ellipticity is lost. Analysis of the azimuthal governing equation yields conclusions relating loss of strict convexity of the considered strain-energy function to the existence of multiple solutions. In par-

ticular, there are in some circumstances three choices for the shear strain, only two of which are admissible. The degree of anisotropy and the geometry of the preferred direction at each point of the body serve to characterize the nature of the surfaces of discontinuity (strong or weak) emerging from the failure of strong ellipticity, which may only happen when the preferred direction undergoes contraction. The surfaces of discontinuity are circular cylinders concentric with the tube. In the special case in which the preferred direction is taken to be radial the azimuthal shear causes extension of the preferred direction for either sense of the shear (and no loss of ellipticity). More generally, we consider a preferred direction that depends on the radius in such a fashion that it extends for positive (anticlockwise) shear, but for which in negative (clockwise) shear it may either extend or contract. In the case of negative shear, the distinction between extension and contraction is dependent on the radial position, the precise disposition of the fibers, the degree of anisotropy and the magnitude of the applied shear stress.

For the same reinforcement, the Varga model is then, in Section 7, chosen to represent the isotropic base material. In this case closed-form solutions are not readily obtainable, and we therefore present numerical results that are parallel to those for the neo-Hookean material. In particular, we again determine a relationship between loss of ellipticity and the existence of non-smooth and multiple solutions that turns out to be very similar to that obtained for the reinforced neo-Hookean model. Unlike the previous case, however, negative shear always leads to ellipticity failure regardless the degree of anisotropy of the considered material.

Finally, several numerical examples are used in Section 8 to illustrate some of the aspects discussed in the foregoing paragraphs, and the overall response of a body undergoing such a deformation is also highlighted. As in the isotropic material case, a unique energy minimizing deformation can be associated with each value of applied shear stress (or twist angle), and deformations containing a surface of discontinuity are confined to a particular interval of this shear stress. However, in contrast to the case of loss of ellipticity in isotropic tubes , certain radial variations of the preferred direction give loss of ellipticity that is always confined to a small region of the tube. This includes cases in which ellipticity can be lost at only a single internal radius and cases in which loss of ellipticity occurs over an interval of internal radii. In the latter case, a surface of discontinuity emerges in the interior of the tube, increases its radius under increasing twist, and then disappears while still strictly interior to the tube.

2. THE AZIMUTHAL SHEAR DEFORMATION

Consider a circular cylindrical tube with reference geometry defined by

$$A \leq R \leq B, \quad 0 \leq \Theta \leq 2\pi, \quad 0 \leq Z \leq L, \tag{1}$$

where (R, Θ, Z) are cylindrical polar coordinates in the reference configuration (assumed free of stress) relative to a cylindrical polar basis $\{\mathbf{E}_I\}$, $I \in \{R, \Theta, Z\}$.

The deformation of *pure azimuthal shear* is defined by

$$r = R, \quad \theta = \Theta + g(R), \quad z = Z, \tag{2}$$

where (r, θ, z) are cylindrical polar coordinates in the deformed configuration associated with the cylindrical polar basis $\{\mathbf{e}_i\}, i \in \{r, \theta, z\}$, and $g(R) = g(r)$ is a function to be determined. We suppose that

$$g(a) = 0, \quad g(b) = \psi, \tag{3}$$

where ψ, which may be positive or negative, is the angle of rotation of the outer boundary $r = b = B$ relative to $r = a = A$.

The deformation gradient tensor, denoted $\mathbf{F}$, has the form

$$\mathbf{F} = \mathbf{R} + \gamma\, \mathbf{e}_\theta \otimes \mathbf{E}_R, \tag{4}$$

where $\mathbf{R} = \mathbf{e}_r \otimes \mathbf{E}_R + \mathbf{e}_\theta \otimes \mathbf{E}_\Theta + \mathbf{e}_z \otimes \mathbf{E}_Z$, while the corresponding left Cauchy–Green tensor, denoted $\mathbf{B}$, is

$$\mathbf{B} = \mathbf{F}\mathbf{F}^{\mathrm{T}} = \mathbf{I} + \gamma\, (\mathbf{e}_r \otimes \mathbf{e}_\theta + \mathbf{e}_\theta \otimes \mathbf{e}_r) + \gamma^2 \mathbf{e}_\theta \otimes \mathbf{e}_\theta, \tag{5}$$

where $\mathbf{I}$ is the identity tensor, $\gamma = rg'(r)$ is the amount of shear (locally a simple shear in the planes normal to $\mathbf{e}_z$), the prime on g indicates differentiation with respect to $r = R$ and $^{\mathrm{T}}$ indicates the transpose (of a second-order tensor).

Let $\mathbf{M}$ be a unit vector, defined in the reference configuration, that identifies locally a preferred direction. In particular, we suppose that $\mathbf{M}$ lies in (R, Θ)-planes, so that we may write

$$\mathbf{M} = M_R \mathbf{E}_R + M_\Theta \mathbf{E}_\Theta, \quad M_R^2 + M_\Theta^2 = 1. \tag{6}$$

The geometrical nature of the preferred direction may be characterized in terms of the *scalar bijection* mapping $G : [A, B] \longrightarrow [0, \Theta_1 - \Theta_0]$ via the equation

$$\Theta = G(R) + \Theta_0, \quad G(A) = 0, \quad G(B) = \Theta_1 - \Theta_0, \tag{7}$$

where $\Theta_0 \in [0, 2\pi]$ and $\Theta_1 - \Theta_0 > 0$ is fixed independently of Θ_0.

Then,

$$M_R = \frac{1}{\sqrt{(RG'(R))^2 + 1}}, \quad M_\Theta = \frac{RG'(R)}{\sqrt{(RG'(R))^2 + 1}}, \tag{8}$$

and $G'(R) = dG(R)/dR$. We assume here that $G'(R) \geq 0$. A schematic of a possible geometrical arrangement of the preferred direction is depicted in Figure 1. Note that M_R and M_Θ are functions of the radius R only. It will sometimes be convenient to identify the preferred direction in terms of the angle $\alpha = \alpha(R)$, with $\alpha \in [0, \pi/2]$ defined by

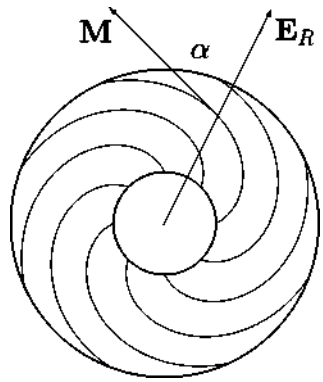

Figure 1. Illustration of a possible arrangement of the preferred direction in the reference configuration according to Equation (7). The angle α is identified by noting that $M_R = \cos\alpha$.

$$\tan\alpha = M_\Theta / M_R = RG'(R). \tag{9}$$

Under the considered deformation $\mathbf{M}$ becomes $\mathbf{m}$, say, which is given by

$$\mathbf{m} = \mathbf{F}\mathbf{M} = M_R\mathbf{e}_r + (M_\Theta + \gamma M_R)\mathbf{e}_\theta. \tag{10}$$

The kinematic invariants of interest for the considered deformation are denoted by I_1 and I_4 and defined by

$$I_1 = \mathrm{tr}\mathbf{B} = 3 + \gamma^2, \quad I_4 = \mathbf{m}\cdot\mathbf{m} = 1 + 2\gamma M_R M_\Theta + \gamma^2 M_R^2. \tag{11}$$

We note that, in general, for an incompressible material (in three dimensions) there are four independent invariants associated with the deformation and the direction $\mathbf{M}$ when no distinction is made between $\mathbf{M}$ and $-\mathbf{M}$. The other two invariants are usually denoted I_2 and I_5. However, in plane strain $I_2 = I_1$ and $I_5 \equiv (\mathbf{Bm})\cdot\mathbf{m} = (I_1 - 1)I_4 - 1$ [10] and it is not necessary to consider these separately from I_1 and I_4. Note that $(11)_2$ reduces to $I_4 = 1 + \gamma^2$ when $\mathbf{M} = \mathbf{E}_R$ ($\alpha = 0$), while $I_4 = 1$ if $\mathbf{M} = \mathbf{E}_\Theta$ ($\alpha = \pi/2$). In the latter case the deformation corresponds to simple shear in the preferred direction.

Since $M_R \geq 0$ (with equality for $G'(R) \to \infty$) and $M_\Theta \geq 0$ then for positive shear ($\gamma > 0$) we have $I_4 \geq 1$ for $R \in [A, B]$. On the other hand, for negative shear ($\gamma < 0$) and $\alpha \neq 0, \pi/2$,

$$I_4 \gtreqless 1 \quad \text{according as} \quad \gamma(\gamma + 2\tan\alpha) \gtreqless 0. \tag{12}$$

Now, for $\gamma < 0$, with $\alpha \neq 0$, it follows from (12) that $I_4 < 1$ for $\gamma > -2\tan\alpha$ and $I_4 > 1$ for $\gamma < -2\tan\alpha$. Note that α may be a constant, a monotonic increasing or decreasing function of R or none of these. If α is a constant then $RG'(R)$ is a constant and the resulting curve is a logarithmic spiral, with $G(R)$ given by

$$G(R) = (\Theta_1 - \Theta_0)\log(R/A)/\log(B/A). \tag{13}$$

Suppose, for illustration, that α is either a constant or an increasing function of $r = R$ and that $|\gamma|$ is a decreasing function of r. In fact, it is shown in Section 5 that if α is constant then the latter condition holds whenever the strong ellipticity condition holds (but otherwise it may or may not hold depending on the material properties and the dependence of α on r). Then, at the inner boundary $r = a$, as γ decreases from zero, I_4 steadily decreases from 1 until it reaches its minimum value at $\gamma = -\tan\alpha$ and then starts to increase. Therefore, due to monotonicity of $|\gamma|$, we have $I_4 < 1$ for $a \le r \le b$ but when $\gamma = -2\tan\alpha$ at the inner boundary, I_4 returns to the value 1, but remains less than 1 for $a < r \le b$. Thereafter, I_4 is greater than 1 at the inner boundary and there is a value of $r \in (a, b)$, denoted r_α, at which $\gamma = -2\tan\alpha$, so that $I_4 > 1$ for $a \le r < r_\alpha$ and $I_4 < 1$ for $r_\alpha < r \le b$. The radial location r_α increases with $|\gamma|$. At sufficiently large $|\gamma|$, r_α reaches the value b and thereafter I_4 is greater than 1 for $a \le r \le b$.

3. CONSTITUTIVE LAW: TRANSVERSE ISOTROPY

For a transversely isotropic incompressible elastic solid, when restricted to the plane strain specialization, the strain-energy function W may be treated in general as a function of I_1 and I_4 alone (see, e.g., Merodio and Ogden) and we write

$$W = \hat{W}(I_1, I_4). \tag{14}$$

The associated in-plane Cauchy stress tensor $\boldsymbol{\sigma}$ then has the form

$$\boldsymbol{\sigma} = -p\mathbf{I} + 2\hat{W}_1\mathbf{B} + 2\hat{W}_4\mathbf{m}\otimes\mathbf{m}, \tag{15}$$

where now $\mathbf{I}$ and $\mathbf{B}$ are the in-plane identity and left Cauchy–Green tensors, respectively, p is the corresponding Lagrange multiplier associated with the incompressibility constraint and $\hat{W}_1 = \partial\hat{W}/\partial I_1$, $\hat{W}_4 = \partial\hat{W}/\partial I_4$.

The (in-plane) cylindrical polar components of $\boldsymbol{\sigma}$ are read off as

$$\sigma_{rr} = -p + 2\hat{W}_1 + 2\hat{W}_4 M_R^2, \tag{16}$$

$$\sigma_{\theta\theta} = -p + 2\hat{W}_1(1+\gamma^2) + 2\hat{W}_4(M_\Theta + \gamma M_R)^2, \tag{17}$$

$$\sigma_{r\theta} = 2\hat{W}_1\gamma + 2\hat{W}_4 M_R(M_\Theta + \gamma M_R), \tag{18}$$

from which it is easy to show that

$$\sigma_{\theta\theta} - \sigma_{rr} = \gamma\,\sigma_{r\theta} + 2\hat{W}_4(\gamma M_R M_\Theta + M_\Theta^2 - M_R^2). \tag{19}$$

In view of (11) and (9) we may now introduce a new function, denoted $\tilde{W}$, such that

$$\tilde{W}(\gamma, \alpha) = \hat{W}(I_1, I_4), \tag{20}$$

and differentiation of (20) yields the simple formula

$$\sigma_{r\theta} = \frac{\partial \tilde{W}}{\partial \gamma} \tag{21}$$

for the shear stress. We note in passing that for any elastic material for which the strain energy can be regarded as a function of the single deformation variable γ for the considered deformation the formula (21) applies. In (20) we should remark that α is a material parameter, not a deformation variable, and its inclusion reflects the fact that the material properties are inhomogeneous if α depends on R. With this in mind we note that the connection (19) can be rewritten in the form

$$\frac{\partial \tilde{W}}{\partial \alpha} = \gamma^2 \sigma_{r\theta} + \gamma\,(\sigma_{rr} - \sigma_{\theta\theta}). \tag{22}$$

4. EQUILIBRIUM EQUATIONS

For the deformation and constitutive law discussed in the foregoing sections the equilibrium equation $\mathrm{div}\boldsymbol{\sigma} = \mathbf{0}$ (in the absence of body forces) has just two non-trivial components, namely the radial equation

$$\frac{\mathrm{d}\sigma_{rr}}{\mathrm{d}r} + \frac{1}{r}(\sigma_{rr} - \sigma_{\theta\theta}) = 0 \tag{23}$$

and the azimuthal equation

$$\frac{\mathrm{d}}{\mathrm{d}r}(r^2 \sigma_{r\theta}) = 0. \tag{24}$$

The azimuthal equation (24) integrates to give, in conjunction with (21),

$$\sigma_{r\theta} \equiv \frac{\partial \tilde{W}}{\partial \gamma} = \frac{\tau_\theta b^2}{r^2}, \tag{25}$$

which, for any given form of $\tilde{W}$, serves to determine γ as a function of r, and hence, via $\gamma = rg'(r)$, the deformation function $g(r)$, subject to the boundary conditions (3). We emphasize that the form of the function $g(r)$ depends on the form of the strain-energy function. The parameter τ_θ in (25) is a constant, representing the value of the azimuthal stress component on the boundary $r = b$. In addition, the quantity $2\pi\tau_\theta b^2$ represents the resultant torque (twisting moment). Either τ_θ or ψ in $(3)_2$ (but not both) can be regarded as providing the boundary condition on $r = b$.

For the isotropic theory, as discussed by Jiang and Ogden , positive γ (i.e. positive ψ) is associated with $\tau_\theta > 0$ while $\gamma < 0$ is related to $\tau_\theta < 0$. This assertion, in conjunction with (25), clearly suggests that

$$\sigma_{r\theta} \equiv \frac{\partial \tilde{W}}{\partial \gamma} \gtreqless 0 \quad \text{according as} \quad \gamma \gtreqless 0. \tag{26}$$

We adopt these restrictions in what follows, and more detailed commentary on them is provided after equation (41).

Once γ is determined, the role of the radial equation (23) is to determine σ_{rr}, or equivalently p. Integration of equation (23), on use of (22) and (25), yields

$$\sigma_{rr}(r) = \sigma_{rr}(a) + \int_a^r \left(g'\tau_\theta b^2 - (g')^{-1} \frac{\partial \tilde{W}}{\partial \alpha} \right) \frac{\mathrm{d}R}{R^2}, \tag{27}$$

in which R is used as the integration variable. Because of the incompressibility constraint the value of $\sigma_{rr}(a)$ is at our disposal. If required, the normal component $\sigma_{\theta\theta}$ can now be obtained from (23).

At this point, it is worth mentioning that, for a transversely isotropic material, unlike the situation in the isotropic theory, Equation (25) might have an alternative role. Specifically, if a certain shear-stress–strain response and distribution is required, then Equation (25) can be used to identify the preferred directions, in other words the components (8) or $G(R)$ itself, for which such a deformation is sustainable. We do not pursue this design idea in the present analysis, however.

5. STRONG ELLIPTICITY AND A CLASS OF REINFORCING MODELS

We now discuss the strong ellipticity condition for the considered azimuthal shear deformation and constitutive law. For this purpose we draw on the general plane strain strong ellipticity condition for transversely isotropic materials given by Merodio and Ogden for a strain-energy function of the form $\hat{W}(I_1, I_4)$. This may be written

$$\begin{aligned} & 2\hat{W}_{11}[\mathbf{n}\cdot(\mathbf{B}\mathbf{a})]^2 + 4\hat{W}_{14}\mathbf{n}\cdot(\mathbf{B}\mathbf{a})(\mathbf{n}\cdot\mathbf{m})(\mathbf{n}\times\mathbf{m})_3 \\ + \quad & 2\hat{W}_{44}(\mathbf{n}\cdot\mathbf{m})^2(\mathbf{n}\times\mathbf{m})_3^2 + \hat{W}_1\mathbf{n}\cdot(\mathbf{B}\mathbf{n}) + \hat{W}_4(\mathbf{n}\cdot\mathbf{m})^2 > 0 \end{aligned} \tag{28}$$

for all in-plane unit vectors $\mathbf{n}$ and $\mathbf{a}$ satisfying $\mathbf{a}\cdot\mathbf{n} = 0$, where $(\mathbf{n}\times\mathbf{m})_3 = n_1m_2 - n_2m_1$, (n_1, n_2) and (m_1, m_2) being the components of $\mathbf{n}$ and $\mathbf{m}$, respectively.

Where ellipticity fails $\mathbf{n}$ defines the normal to the associated (weak or strong) surface of discontinuity. While the inequality (28) is local, for the present problem we have to consider the global implications of the constraints imposed by the geometry. If the circular geometry is to be maintained then any surface of discontinuity is necessarily constrained to be circular cylindrical and concentric with the tube. Thus, we may take $\mathbf{n} = \mathbf{e}_r$ and $\mathbf{a} = \mathbf{e}_\theta$. Then,

$\mathbf{n}\cdot(\mathbf{Bn}) = 1$, $(\mathbf{n}\times\mathbf{m})_3 = (M_\Theta + \gamma M_R)$, $\mathbf{n}\cdot(\mathbf{Ba}) = \gamma$, $\mathbf{n}\cdot\mathbf{m} = M_R$, and (28) therefore reduces to

$$2\hat{W}_{11}\gamma^2 + 4\hat{W}_{14}\gamma M_R(M_\Theta + \gamma M_R) + 2\hat{W}_{44}M_R^2(M_\Theta + \gamma M_R)^2 + \hat{W}_1 + \hat{W}_4 M_R^2 \equiv \frac{1}{2}\tilde{W}_{\gamma\gamma} > 0,$$

where a subscript γ signifies the partial derivative $\partial/\partial\gamma$. Thus, for the considered problem, strong ellipticity is equivalent to the simple inequality $\tilde{W}_{\gamma\gamma} > 0$, and loss of ellipticity therefore occurs, if at all, at a value of r for which $\tilde{W}_{\gamma\gamma} = 0$.

Expressed otherwise, strong ellipticity is equivalent to the strain-energy function being a strictly locally convex function of γ. Thus,

$$\tilde{W}_{\gamma\gamma} \equiv \frac{\partial\sigma_{r\theta}}{\partial\gamma} > 0. \tag{29}$$

This is easily confirmed in the case of an isotropic material, for which we write (14) as $\hat{W} = E(I_1)$. Then, necessary and sufficient conditions for (28) are [10, 12]

$$2(I_1 - 3)E''(I_1) + E'(I_1) > 0, \quad E'(I_1) > 0. \tag{30}$$

But, since $I_1 = 3 + \gamma^2$, we introduce the notation $\tilde{E}(\gamma)$ defined by $\tilde{E}(\gamma) = E(I_1)$. The inequalities (30) then become

$$\tilde{E}''(\gamma) > 0, \quad \tilde{E}'(\gamma) \gtreqless 0 \quad \text{for} \quad \gamma \gtreqless 0. \tag{31}$$

Note, however, that the latter is equivalent to the adopted condition (26), and hence, for isotropic materials, the remaining strong ellipticity condition is simply $\tilde{E}''(\gamma) > 0$.

It should be emphasized that for the deformation under examination, and as for the isotropic theory [2], the ellipticity requirement (29), if it holds for all γ, ensures, for any given τ_θ, uniqueness of the solution of (25) for γ provided the growth condition $\tilde{W}_\gamma \to \infty$ as $\gamma \to \infty$ holds. Loss of ellipticity is therefore closely related to loss of uniqueness of the solution for γ.

Finally in this section, we note that

$$\tilde{W}_{\gamma\gamma}\frac{\mathrm{d}\gamma}{\mathrm{d}r} + \tilde{W}_{\gamma\alpha}\frac{\mathrm{d}\alpha}{\mathrm{d}r} = -2\frac{\tau_\theta b^2}{r^3}, \tag{32}$$

and recall that by (25) and (26) τ_θ has the same sign as γ. This shows that if (29) holds and if α is independent of r then $\mathrm{d}\gamma/\mathrm{d}r \gtreqless 0$ according as $\tau_\theta \gtreqless 0$. Thus, $|\gamma|$ is a decreasing function of r whenever strong ellipticity holds. If α depends on r then, in general, whether or not $|\gamma|$ is monotonic depends both on the nature of this dependence and on how $\tilde{W}$ depends on α. An example of non-monotonicity is illustrated in Section 8.2.

In order to examine loss of ellipticity in detail we focus attention on two particular strain-energy functions within the general class characterized by the separable form

$$\hat{W}(I_1, I_4) = E(I_1) + F(I_4), \tag{33}$$

in which the first term $E(I_1)$ represents the isotropic base material and the additional term $F(I_4)$ represents the reinforcement associated with the transversely isotropic nature of the considered materials, the invariant I_4 being associated with the preferred direction $\mathbf{M}$. Several authors (see, for example, Merodio and Ogden and references therein) have considered a decomposition of the form (33), or specializations thereof, where, in each case, the reinforcing contribution $F(I_4)$ has been taken to satisfy

$$F'(I_4) > 0\,(< 0) \quad \text{for} \quad I_4 > 1\,(< 1), \qquad F'(1) = 0. \tag{34}$$

These conditions ensure that the contribution of $F(I_4)$ to the component of the Cauchy stress tensor (15) in the deformed preferred direction is positive (negative) under extension (contraction) of the preferred direction.

It is useful in what follows to examine certain properties of the energy function $\hat{W}(I_1, I_4)$ specified in (33) in respect of its dependence on γ and to write

$$\tilde{W}(\gamma) = \tilde{E}(\gamma) + \tilde{F}(\gamma), \tag{35}$$

dropping the explicit dependence on α. It is similarly convenient to use the notation $\sigma_{r\theta} = s(r)$ so as to emphasize the dependence of the shear stress on r, whence, from (25),

$$\frac{\tau_\theta b^2}{r^2} = s(r) = \tilde{E}'(\gamma) + \tilde{F}'(\gamma). \tag{36}$$

We emphasize that for a strain-energy function of the form (33) satisfying (34), the properties of $\tilde{E}(\gamma)$ have to be consistent with (26), where in general $\tilde{E}(\gamma)$ need not be a convex function. However, we restrict attention henceforth to conventional isotropic base material functions. Much more detail on the possibilities for loss of ellipticity due to the properties of $\tilde{E}(\gamma)$ and $\tilde{F}(\gamma)$ can be gleaned from the work of Merodio and Ogden .

6. THE REINFORCED NEO-HOOKEAN MODEL

In this section we examine in detail the ellipticity status of the neo-Hookean isotropic material augmented with the so-called standard reinforcing model under the pure azimuthal shear deformation. In particular, the breakdown of strong ellipticity and loss of strict local convexity of $\tilde{W} = \hat{W}$ are associated here with the existence of non-unique solutions of the boundary-value problem.

Equation (33) is now specialized to

$$\hat{W}(I_1, I_4) = \frac{1}{2}\mu\left[I_1 - 3 + \rho(I_4 - 1)^2\right], \tag{37}$$

so that

$$E(I_1) = \frac{1}{2}\mu(I_1 - 3), \quad F(I_4) = \frac{1}{2}\mu\rho(I_4 - 1)^2, \tag{38}$$

where the constant μ (> 0) represents the shear modulus of the isotropic base material and ρ (> 0) is a material constant that characterizes the degree of anisotropy associated with the presence of the preferred direction. For the considered deformation we have

$$I_1 - 3 = \gamma^2, \quad I_4 - 1 = \gamma \cos\alpha(2\sin\alpha + \gamma \cos\alpha). \tag{39}$$

It follows that

$$\tilde{W}_\gamma = \mu\gamma \left(2\rho \cos^4\alpha\, \gamma^2 + 6\rho \cos^3\alpha \sin\alpha\, \gamma + 4\rho \cos^2\alpha \sin^2\alpha + 1\right), \tag{40}$$

and it is then easy to show that the inequalities (26) hold if and only if

$$\rho \sin^2 2\alpha < 8. \tag{41}$$

Although the inequalities (26) could be relaxed to provide an alternative route to loss of ellipticity, here we assume that they hold and that loss of ellipticity is associated solely with the condition $\tilde{W}_{\gamma\gamma} = 0$. The restriction (41) on the parameter ρ and the angle α reflects the very special choice of strain-energy function.

More specifically, as discussed in [8] (see Figure 12 therein), $\rho > 8$ offers the possibility that shearing with respect to a particular range of reinforcing orientations gives a resolved shear stress with opposite sign to that of the amount of shear. Similar phenomena are noted and would likely render the considered radially symmetric solutions unstable with respect to more general deformations that are beyond the scope of this article. Here attention is restricted to (41), and more generally (26), so as to justify exclusive focus on the pure azimuthal shear deformations (2).

We remark that to the extent that the transverse isotropy studied here is associated with fiber reinforcement, constancy of the reinforcing parameter ρ might be regarded as associated with a constant fiber density (independent of r). More generally, however, one could consider ρ to depend on r and the subsequent analysis given in the present paper for constant ρ could provide a point of entry for the consideration of any such generalization.

6.1. Multiple Solutions

Here we investigate the existence of multiple solutions of the azimuthal equilibrium equation (25) for γ for given values of the applied shear loading τ_θ. For this purpose it is convenient to use the notations defined by

$$\sigma(\gamma) = \tilde{W}_\gamma/\mu, \quad \tau(r) = s(r)/\mu = \tau_\theta b^2/\mu r^2. \tag{42}$$

In respect of (37), equation (25) yields the cubic

$$\sigma(\gamma) \equiv 2\rho M_R^4 \gamma^3 + 6\rho M_R^3 M_\Theta \gamma^2 + (4\rho M_R^2 M_\Theta^2 + 1)\gamma = \tau(r) \tag{43}$$

for γ. An immediate useful observation is that both $\gamma = -\tan\alpha$ and $\gamma = -2\tan\alpha$ cause the reinforcing term in (43) to vanish, thus yielding $\sigma = \tau = \gamma$ for these two special values of γ. For $\gamma = -2\tan\alpha$, in which case $I_4 = 1$, this correspondence is a consequence of $F'(1) = 0$ in (34). For $\gamma = -\tan\alpha$ it is a consequence of $\partial I_4/\partial\gamma = 0$, which in turn renders $\tilde{F}'(\gamma) = 0$.

In the special case $M_R = 0$, equation (43) yields $\gamma = \tau(r)$ and the solution is exactly that arising in the isotropic theory, i.e. the anisotropy has no influence, either for positive or negative $\tau(r)$. Henceforth, we assume $M_R \neq 0$ ($\alpha \neq \pi/2$).

If $\tau_\theta > 0$ then $\tau(r) > 0$ and, according to (26), we must have $\gamma > 0$, in which case the left-hand side of (43) is a monotonic increasing function of γ, $\tilde{W}$ is a locally strictly convex function of γ and the strong ellipticity condition holds. Hence, (43) yields a unique value for γ. We shall not pursue discussion of this case.

The situation of particular interest is when $\tau_\theta < 0$ so that $\tau(r) < 0$ and, by (26), $\gamma < 0$. First, it is easy to show that if $\rho\sin^2 2\alpha < 2$ then the left-hand side of equation (43) is again a monotonic increasing function of γ. Hence (43) has a unique negative solution, $\gamma = \gamma_1$ say, defined for all $M_R \in (0, 1]$ (and all $r \in [a, b]$). This solution is given explicitly by

$$\gamma_1 = -\tan\alpha + \frac{6^{-2/3}Q^2 - 6^{-1/3}\rho M_R^4(1 - 2\rho M_R^2 M_\Theta^2)}{\rho M_R^4 Q}, \tag{44}$$

for all $a \leq r \leq b$ with $M_R \in (0, 1]$ and for any value of $\tau = \tau(r) < 0$ with real $Q \equiv Q(r)$ being given by

$$\begin{aligned} Q^3 &= 9\rho^2 M_R^7(\tau M_R + M_\Theta) \\ &+ 3^{1/2}\rho^{3/2}M_R^6\sqrt{27\rho M_R^2(\tau M_R + M_\Theta)^2 + 2(1 - 2\rho M_R^2 M_\Theta^2)^3}. \end{aligned} \tag{45}$$

Note that when $\rho = 2$ and $\alpha = \pi/4$ equation (43) simplifies to $(\gamma + 1)^3 = \tau + 1$, and hence $\gamma = \gamma_1 = -1 + (\tau + 1)^{1/3}$. This is negative for $\tau < 0$ and yields the same result as the specialization of (44) with (45).

For $a \leq r \leq b$, the (unique) deformation function, $g_1(r)$ say, is determined by integration of the equation $rg_1'(r) = \gamma_1$ with the boundary conditions (3).

Second, for $\tau < 0$, loss of uniqueness of solution of (43) may occur when $\rho\sin^2 2\alpha$ exceeds the value 2. Then, independently of the magnitude of $\tau < 0$, γ is again given by (44), but only for values of r for which

$$\text{either} \quad 0 < M_R < M_1 \quad \text{or} \quad M_2 < M_R \leq 1, \tag{46}$$

where

$$M_1 = \sqrt{\left(\rho - \sqrt{\rho^2 - 2\rho}\right)\Big/ 2\rho}, \quad M_2 = \sqrt{\left(\rho + \sqrt{\rho^2 - 2\rho}\right)\Big/ 2\rho}. \tag{47}$$

The formula for y_1 is also valid when $M_R = Mi$ or $M_R = M_2$, including the special case r = — tan a, for which y_x = — tan a is a triple root.

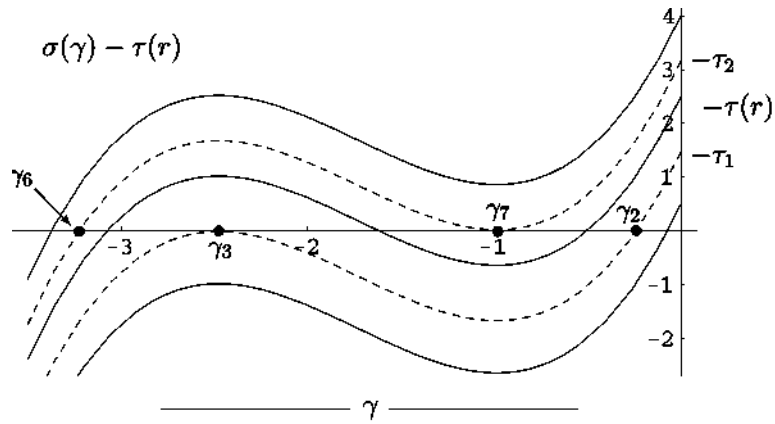

Figure 2. Plot of the cubic *a(y) — z(r)* from (43) against *y* for different values of *z(r):* from bottom to top, *z(r)* > *z1, z(r)* = *%i* (lower dashed curve), r_2 < *z(r)* < *z1, z(r)* = *z2* (upper dashed curve), *z(r)* < r_2. The values *y 2, y3, y 6, y7* are identified by the • symbol, while *yt,y4,y5* are ordered according to 7 5 < 7 3 , 7 3 < 7 4 < 7 7 , 7 7 < 7 i <0. Note that W_{yy} < 0 for y_3 < y <y_7.

Non-uniqueness of the roots y for r < 0 is possible only if/? > 2 and only for values of r such that *p* $\sin^2$ *2a* > *2,* or equivalently

$$M_1 < M_R < M_2, \tag{48}$$

which is, in fact, anticipated on the basis of equation (4.16)

We now consider the effect of increasing the magnitude of the shear stress r^ on the boundary r = *b,* or equivalently of *r(b)* = r_d*/fi.* In Figure 2 we plot, for a series of given values of r(r), the function <r(y) — r(r) against y, where <r(y) is defined in (43). Since *a* (0) = 0 the intercept on the vertical axis is —r (r).

For small values of |r(r)| the equation <r(y) — r(r) =0 clearly has a single solution, which is the value y_1 identified in (44). As |r (r) | increases a second solution of (43) emerges when the curve (the lower dashed curve in Figure 2) just touches the horizontal axis. At this point the two roots for y , denoted y_2 and y_3, are given by

$$y_2 \qquad -\tan\alpha + \frac{\sqrt{6}\sqrt{2\rho M_R^2 M_\Theta^2 - 1}}{3\sqrt{\rho} M_R^2}, \tag{49}$$

$$y_3 \qquad -\tan\alpha - \frac{\sqrt{6}\sqrt{2\rho M_R^2 M_\Theta^2 - 1}}{6\sqrt{\rho} M_R^2}. \tag{50}$$

The value y_2 is the specialization of y_1; while y_3 is the double root associated with the maximum point on the curve.

The corresponding value of z (r) at this point is denoted z i and is given by

$$\tau_1 = -\tan\alpha + \frac{\sqrt{6\rho\left(2\rho M_R^2 M_\Theta^2 - 1\right)^3}}{9\rho M_R^2}. \tag{51}$$

Note that, in general, α depends on r and so, therefore, does the value τ_1.

As $|\tau(r)|$ increases further then three distinct real roots for γ are obtained. However, Q in (45) is now complex and some manipulations are required to rewrite (44) in the simplified form

$$\gamma_1 = -\tan\alpha + \frac{6^{-2/3}}{\rho M_R^4}(Q + \bar{Q}), \tag{52}$$

where $\bar{Q}$ is the complex conjugate of Q. The other two (real) roots, denoted γ_4 and γ_5, are given similarly by

$$\gamma_4 = -\tan\alpha - \frac{6^{-2/3}}{2\rho M_R^4}\left[Q + \bar{Q} - \mathrm{i}\sqrt{3}(Q - \bar{Q})\right], \tag{53}$$

$$\gamma_5 = -\tan\alpha - \frac{6^{-2/3}}{2\rho M_R^4}[Q + \bar{Q} + \mathrm{i}\sqrt{3}(Q - \bar{Q})]. \tag{54}$$

It is convenient to label these two roots so that $\gamma_5 \leq \gamma_4 (< 0)$, noting that they are both equal to γ_3 when $\tau(r) = \tau_1$. Then, with reference to Figure 2, it is easy to show that for $\tau_2 < \tau(r) < \tau_1$, the following orderings hold: $\gamma_5 < \gamma_3 < -\tan\alpha\ (< 0)$, $\gamma_3 < \gamma_4\ (< 0)$. These imply that $\gamma_5 + \tan\alpha < 0$ (and hence $Q + \bar{Q} > 0$), while $\gamma_4 + \tan\alpha$ may be either positive or negative.

The roots γ_1 and γ_4 merge when $\tau(r)$ reaches the value τ_2 given by

$$\tau_2 = -\tan\alpha - \frac{\sqrt{6\rho(2\rho M_R^2 M_\Theta^2 - 1)^3}}{9\rho M_R^2}, \tag{55}$$

which corresponds to the upper dashed curve in Figure 2 and depends on r if α does. The two roots in this case, denoted γ_6, γ_7, are given by

$$\gamma_6 = -\tan\alpha - \frac{\sqrt{6}\sqrt{2\rho M_R^2 M_\Theta^2 - 1}}{3\sqrt{\rho} M_R^2}, \tag{56}$$

$$\gamma_7 = -\tan\alpha + \frac{\sqrt{6}\sqrt{2\rho M_R^2 M_\Theta^2 - 1}}{6\sqrt{\rho} M_R^2}. \tag{57}$$

The (double) root γ_7 is the specialization of γ_1 (and γ_4) for this case and γ_6 is the most negative root. Note that for $\tau_2 < \tau(r) < \tau_1$ we have $\gamma_4 < \gamma_7 < \gamma_1\ (< 0)$, $\gamma_6 < \gamma_5$ and $\gamma_7 + \tan\alpha > 0$, while for $\tau(r) < \tau_2$ there is again only one real root for γ, which we label as $\gamma_5\ (< \gamma_6)$. We note in passing that γ_2 and γ_6 correspond to the same value of I_4, which

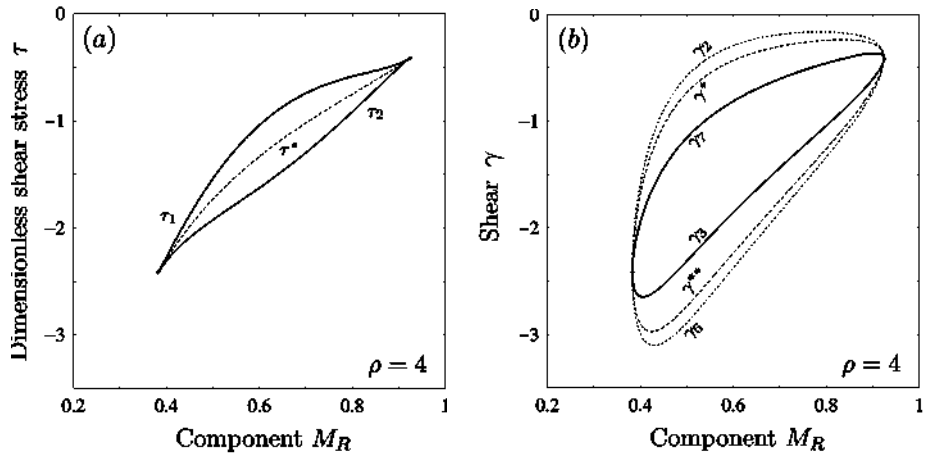

Figure 3. *(a)* Plots of the critical values $x\backslash$ (upper curve) and r_2 (lower curve) against M_R in (M_R, z) space for $p = 4$; *(b)* plots of the critical values y_2, y_6 (dotted curves) and y_3,y_7 (continuous curves) in $\{M_R, y)$ space forp $=4$. The dashed curves and the symbols z^*, y^*,y'' are identified in Section 6.3.

may be written $1 - \gamma_2\gamma_6\cos^2\alpha$. Similarly, for γ_3 and γ_7 we have $I_4 = 1 - \gamma_3\gamma_7\cos^2\alpha$. Moreover, I_4 is less for γ_3 than for γ_2. Note that $\gamma_6 > -2\tan\alpha$ provided (41) holds.

Since τ and (in general) α depend on r the above results are purely local, i.e. they apply for fixed values of r. While $|\tau|$, as defined in (42), is a decreasing function of r, neither τ_1 nor τ_2 is in general a monotonic function of α. Thus, the disposition of possible shear strains for $r \in (a, b)$ can be quite complex. To illustrate to possibilities we show, in Figure 3(a), the nature of the values τ_1 and τ_2 defined by (51) and (55), respectively, as functions of M_R. In Figure 3(b) the corresponding values γ_2, γ_3 and γ_6, γ_7 are shown, in each case for $\rho = 4$. If α is a monotonic increasing (decreasing) function of r, and therefore M_R monotonic decreasing (increasing), the curves in Figure 3 can be interpreted as illustrating qualitatively the dependence of these values on the radius r.

Clearly, the values τ_1 and τ_2 are critical for determining the existence of multiple values for y and hence non-unique continuous deformation fields $g(r)$ in (2). For $\tau(r)$ between τ_1 and τ_2, non-uniqueness is possible. Subject to the restriction $\rho\sin^2 2\alpha < 8$, an increase in the parameter $\rho > 2$ corresponds to expansion of the domain where non-uniqueness of y is possible since τ_1 is a monotonic increasing function and τ_2 a monotonic decreasing function of ρ. In comparison with Figure 3, Figure 4 shows corresponding results for $\rho = 9$. For this value of ρ we have to ensure that the inequality (41) is satisfied. It is provided $M_R < \sqrt{3}/3 \approx 0.577$ or $M_R > \sqrt{6}/3 \approx 0.817$. In Figure 4(a) the τ_1 curve cuts the axis $\tau = 0$ at the values $M_R = \sqrt{3}/3, \sqrt{6}/3$ and the interval $M_R \in [\sqrt{3}/3, \sqrt{6}/3]$ is therefore excluded from consideration. This applies equally in Figure 4(b), which, for the same interval, reveals inadmissible values for y, denoted γ_4^* and γ_5^*, that are obtained from the formulas (53) and (54) for γ_4 and γ_5 with (45) for $\tau = 0$. Note that τ_1 is not here a monotonic function of M_R.

We remark that, for a certain range of values of $\rho > 2$, τ_1 is monotonically increasing in the component M_R, as is evident in the example in Figure 3. This means that loss of

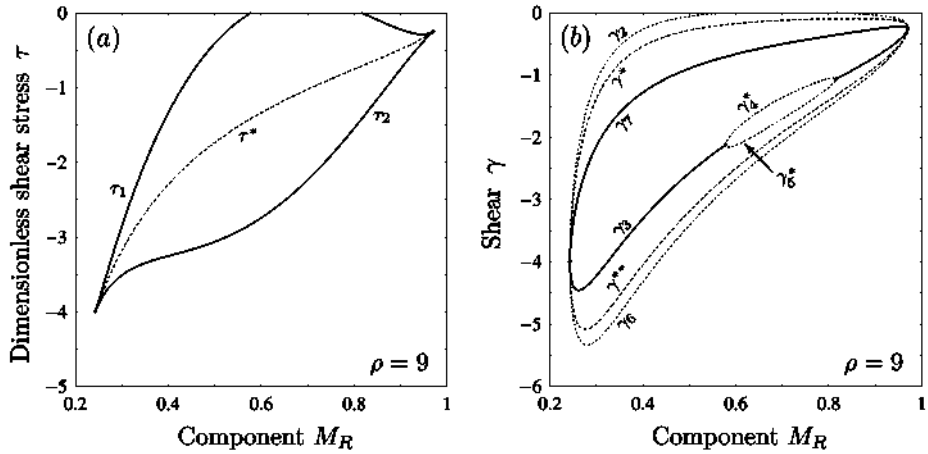

Figure 4. (a) Plots of the critical values τ_1 (upper curve) and τ_2 (lower curve) against M_R in (M_R, τ) space for $\rho = 9$; (b) plots of the critical values γ_2, γ_6 (dotted curves) and γ_3,γ_7 (continuous curves) in (M_R, γ) space for $\rho = 9$. The interval $M_R \in [V3/3, V6/3]$ is excluded since the inequality (41) is violated. The inadmissible shear strains γ_1 and γ_1 are within this interval. The dashed curves and the symbols τ^*, γ^*, γ^{**} are identified in Section 6.3.

uniqueness is initiated for points with M_R close to M_2 since the latter is associated with the minimum possible value of $|\tau_1|$. More specifically, when ρ exceeds the approximate value 5.39, τ_1 loses its monotonic character; however, the least value of $|\tau|$ for which loss of uniqueness first occurs is still close to $M_R = M_2$ until ρ reaches the approximate value 6.19. Thereafter, multiplicity of choices for γ first occurs away from M_2, and, in particular, for $M_R \approx 0.764 < M_2 \approx 0.956$, while any further increase in ρ results in a decrease in the value of M_R for which $|\tau_1|$ is minimized.

The dashed curves in Figures 3 and 4 have a special significance, which will be discussed in Section 6.3.

In order to simplify the discussion of multiplicity, we now focus on the case in which a is independent of r. Then, τ_1 and τ_2 are also independent of r, and, with reference to Figure 2, we may determine the effect of increasing $|\tau(r)|$ as follows.

We note that $|\tau(r)|$ has its largest value at $r = a$. For $0 > \tau(a) > \tau_1$ there is a unique value $\gamma = \gamma_1$ that applies for $a \leq r \leq b$. For $\tau(a) = \tau_1$ this value $(= \gamma_2)$ again applies for $a \leq r \leq b$, but a second value γ_3 becomes possible at $r = a$. For $\tau(b) > \tau_1 > \tau(a) > \tau_2$, three values are possible, corresponding to the intercepts of the central curve in Figure 2 with the horizontal axis. These are γ_1 in (52) and γ_4 and γ_5 in (53) and (54), respectively, labelled so that $\gamma_5 < \gamma_4 < \gamma_1$. There is then a value of $r \in (a, b)$, r^* say, such that $\tau(r^*) = \tau_1$. For $r > r^*$ the value γ_1 is the only one possible, but for $r < r^*$ three values, namely γ_1, γ_4 and γ_5, are possible. As we shall discuss further in Section 6.3, any use of the choice γ_4 in the construction of the function $g(r)$ gives rise to an energetically unstable deformation by all conventional stability criteria. Hence the choice γ_4 will not be admitted. Thus, for $r < r^*$ only the two values γ_1 and γ_5 are admissible. Even so, the possibility of γ having a jump from γ_1 to γ_5 arises, whereupon the determination of the point or points at which

such a jump occurs requires further discussion. This will also be provided in Section 6.3 in relation to the stability status of the different values of γ. Such jumps are called *elastostatic shocks* and, in the context of fiber reinforced materials, are referred to as *kink surfaces*. With further increase in $|\tau_\theta|$, the possibility of two admissible values of γ is retained provided $\tau(b)$ reaches the value τ_1 before $\tau(a)$ reaches the value τ_2. If, however, $\tau(a)$ reaches τ_2 before $\tau(b)$ reaches τ_1 a further increase in τ_θ will generate two circles, of radii r^* and $r^{**} < r^*$, say, such that there is only a single value (γ_5) for $a < r < r^{**}$, two admissible values (γ_1 and γ_5) for $r^{**} < r < r^*$ and only one (γ_1) for $r^* < r < b$.

The situation described above mirrors that studied by Abeyaratne in the context of the isotropic problem with a non-monotone shear stress response function. As shown for the isotropic material problem, it will generally be the case that smooth solutions will not exist for certain values of ψ, which in turn motivates the explicit need for deformations involving such a discontinuity surface. Once such elastostatic shock solutions are admitted, one then typically obtains a multiplicity of solutions for certain values of ψ whereupon the issue of selecting solutions of physical significance becomes central to further progress. As elaborated in Section 6.3 we shall here follow by invoking an absolute stability selection criterion that essentially selects global energy minimizers within the class of azimuthal shear deformations (2). As discussed further in what follows, such solutions have an equivalent interpretation of dissipation free shock motion when the problem is viewed quasi-statically for a time varying ψ. , an immediate consequence is that a unique solution $g(r)$, which may or may not involve an elastostatic shock, follows for each value ψ and the same solution is obtained for the quasi-static interpretation of the problem irrespective of whether ψ is increasing or decreasing. Indeed, Abeyaratne provides full details for associating any boundary value ψ to such a solution for the isotropic problem. In the present paper we do not provide the same focus on mapping the boundary value ψ onto solutions and instead refer the reader to [6] for more detail on how to treat this aspect of the problem. This allows us to retain our focus on the new issues pertaining to the effect of the fiber reinforcement associated with transverse isotropy.

The possibilities just described are reflected in Figure 3, for example. For values of M_R between $M_1 = (\sqrt{2-\sqrt{2}})/2 \approx 0.383$ and $M_2 = (\sqrt{2+\sqrt{2}})/2 \approx 0.924$ (for $\rho = 4$), we see that as τ decreases from zero there is initially one value for γ, namely $\gamma_1 > \gamma_2$. Two values, γ_2 and γ_3, become possible when τ reaches τ_1. As τ decreases further, three values of γ become possible: one (γ_1) is found between γ_2 and γ_7, a second (γ_4) between γ_7 and γ_3 and a third (γ_5) between γ_3 and γ_6. The value γ_4, as mentioned already, is not admissible. After τ reaches τ_2 (and γ reaches γ_7) there is again uniqueness. Thus, with reference to Figure 3(b), we see that outside the closed curve defined by γ_2 and γ_6 the value of γ is uniquely determined, while inside this curve two admissible choices (γ_1 and γ_5) are possible.

In constructing any such discontinuity surface across which the shear strain γ jumps between γ_1 and γ_5 it is to be remarked that there is no associated change in the value of τ_θ even though τ_θ appeared originally as an integration constant in (25). Continuity of τ_θ is necessary for continuity of $\sigma_{r\theta}$. Continuity of σ_{rr} follows from (27), which in turn ensures traction continuity across the discontinuity surface.

The case $a = 0$. Finally in this section, we consider the exceptional case for which the preferred direction is taken to be radial for r e $[a, b]$, i.e. $a = 0$. Then y may be computed from (44) for any r (positive or negative) and $p > 0$, whilst (45) reduces to

$$Q^3 = 9\rho^2\tau + \sqrt{81\rho^4\tau^2 + 6\rho^3}. \tag{58}$$

After some manipulation it can be shown that $\gamma = \gamma_1$ has the form

$$\gamma_1 = \frac{6^{1/3}\rho\tau}{q_+^{2/3} + q_-^{2/3} + 6^{1/3}\rho}, \tag{59}$$

where $q_\pm = \sqrt{81\rho^4\tau^2 + 6\rho^3} \pm 9\rho^2\tau$. The antisymmetry of γ_1 with respect to the change of sign of τ is then apparent. The equation $rg_1'(r) = \gamma_1$ is solved to give

$$g_1(r) = L(r) - L(a) \tag{60}$$

for $a \le r \le b$, where

$$\sqrt{2\rho}\, L(r) = -\frac{\sqrt{3}}{2}(x - x^{-1}) + \tan^{-1}\left(\frac{x - x^{-1}}{\sqrt{3}}\right), \tag{61}$$

x (> 0) is defined by $x = Q/(6\rho^3)^{1/6}$, $Q > 0$, and we recall that $\tau = \tau_\theta b^2/\mu r^2$.

6.2. *Loss of Ellipticity*

The loss of uniqueness discussed in the foregoing section is closely related to loss of ellipticity, and the connection will be elaborated in the present section. Strict local convexity of $\tilde{W} \equiv \hat{W}$ as a function of γ is equivalent to the strong ellipticity condition $\tilde{W}_{\gamma\gamma} > 0$, and for the considered reinforced neo-Hookean model (37) this yields

$$6\rho M_R^4\gamma^2 + 12\rho M_R^3 M_\Theta\gamma + 4\rho M_R^2 M_\Theta^2 + 1 > 0. \tag{62}$$

This holds for $\gamma > 0$, while for it to hold for all γ it is necessary and sufficient that

$$\rho \sin^2 2\alpha < 2. \tag{63}$$

Thus, bearing in mind the restriction (41), failure of ellipticity requires

$$2 \le \rho \sin^2 2\alpha < 8. \tag{64}$$

Note, in particular, that the left-hand inequality in (64) cannot hold unless $\rho \ge 2$. For $\rho = 2$ only equality can hold and it requires that $\alpha = \pi/4$.

Failure of the inequality (62) can occur for those r for which $M_1 \le M_R \le M_2$ and only when γ is such that $\gamma_3 \le \gamma \le \gamma_7$. In particular, $\tilde{W}_{\gamma\gamma} = 0$ for $\gamma = \gamma_3$ and $\gamma = \gamma_7$,

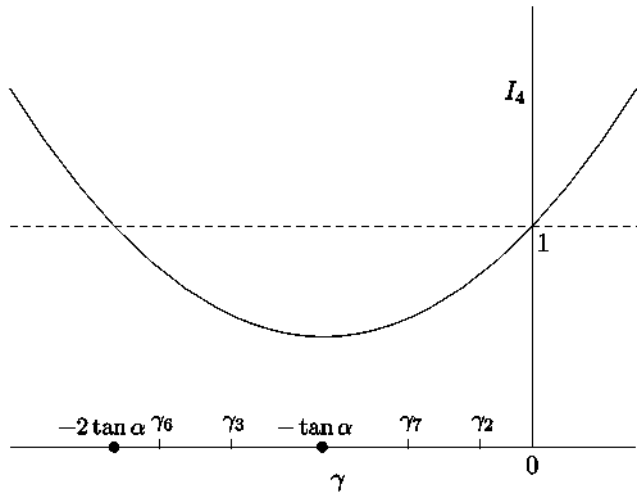

Figure 5. Plot of the invariant I_4 against y showing the relative positions of y_2, y_3, y_6, y_1. The value $I_4 = 1$ is shown as the dashed line, which cuts the I_4 curve at $y = -2\tan a$. The minimum of I_4 occurs at $y = -\tan a$. The values $-\tan a$ and $-2\tan a$ are indicated by the symbol • on the y axis.

which correspond to $r = x_x$ and $r = r_2$, respectively. Thus, the emergence of a second value for y when $r = x\backslash$ coincides with loss of ellipticity. For the case of constant a, as $|r|$ increases ellipticity fails first on $r = a$ and thereafter on a circle of radius $r = r^*$, which increases until $r = b$ is reached. The (unique) value y_x applies for $r^* < r < b$, while for $a < r < r^*$ an alternative value is possible, i.e. y_1 can jump to y_5. For each of y_1 and y_5 strong ellipticity holds (i.e. the slope of the central curve in Figure 2 is positive for each of these values). The middle value y_4 is not admissible since at this point $W_{yy} < 0$, i.e. it is unstable. Indeed, $W_{yy} < 0$ for $y_3 < y < y_7$, as can be seen in Figure 2. For the model under examination, loss of uniqueness of the solution of (43) for $y < 0$ implies failure of strong ellipticity, but the converse is not true in general since, for $p \sin^2 2a = 2$, the roots for y all coincide at a horizontal point of inflection ($y = -\tan a$). Such a situation corresponds to a weak discontinuity, with y continuous but dy /dr discontinuous at the value of r in question. This can happen only for $M_R = Mi$ or $M_R = M_2$ with $y_3 = y_7 = -\tan a$ ($= r! = r_2$).

We now examine the ellipticity status in terms of the invariant U since it is clear that breakdown of ellipticity is always associated with $I_4 < 1$. The relative placements of the values y_6, y_3, y_7, y_2 are shown in Figure 5 together with a plot of the invariant U as a function of y . For the considered material model and deformation, $W_{yy} < 0$ for $y_3 < y < y_7$, and $7_4 < 1$ for all r for which $y^\wedge,<y < y_7$ holds. On the other hand, $U < 1$ does not, in general, imply $W_{yy} < 0$. Indeed, $W_{yy} > 0$ for either $-2\tan a < y < y_3$ or $y_7 < y < 0$, for which intervals $U < 1$.

Thus, it is generally the case that if loss of ellipticity takes place it will first occur before I_4 reaches its minimum value. The exception is for the non-generic situation in which $y_7 = yA = 73 = -\tan a$, corresponding to $M_R = Mi = M_2$. In such a situation, any subsequent change in the boundary condition generally causes I_4 to cease to be at its minimum value, whereupon ellipticity is regained. An example of this transient loss of ellipticity is presented

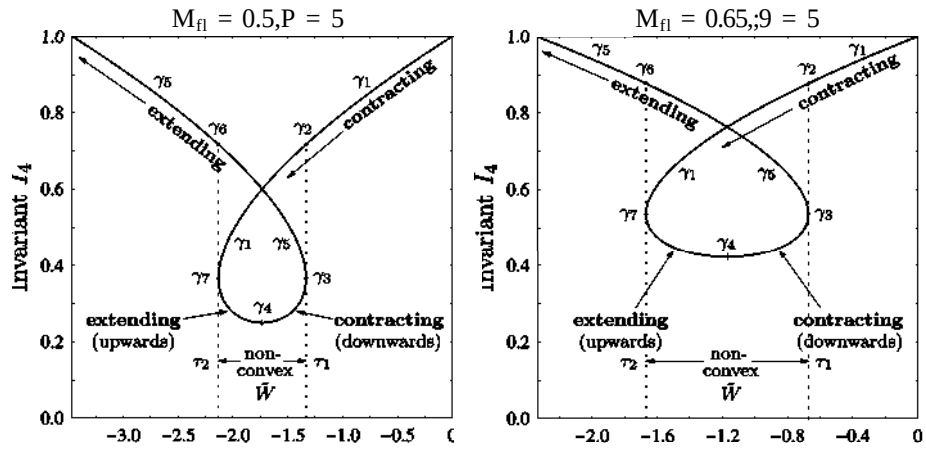

Figure 6. Plots of the invariant I_4 against r < 0 for M_R = 0.5, 0.65 with p = 5 showing the locations of the different y values. Note that y_4 is located in the region of non-convex W.

in Section 8.2. In Figure 6, for $\rho = 5$ and $M_R = 0.5, 0.65$, the dependence of $I_4 \leq 1$ on $\tau \leq 0$ is plotted, with the locations of the different values for y identified.

6.3. Energy Minimal Solutions

Consider a programme of loading such that σ and correspondingly y decreases from zero. For $-\sigma < -\tau_1$, as we have seen, there is only one solution of (43) for y, namely the root y_1. We focus on the values of σ such that $-\tau_1 < -\sigma < -\tau_2$, when there are two roots, y_1 and $y_5 < y_1$. With reference to Figure 7, let τ^* be the value of σ for which the horizontal line $\sigma = \tau^*$ cuts the σ curve to form two closed regions with equal areas. This is, of course, the well-known Maxwell line. Let y^* and $y^{**} < y^*$ be the corresponding values of y_1 and y_5. The Maxwell line is therefore defined by the equality (namely Equations (3.2)–(3.4))

$$\tilde{W}(y^{**}) - \tilde{W}(y^*) - \tau^*(y^{**} - y^*) = 0. \tag{65}$$

The dashed curves in Figures 3(a) and 4(a) are plots of the relevant values of T* for the examples therein against M_R, and in Figures 3(b) and 4(b) the associated curves of y * and y ** are shown.

For solutions containing a discontinuity surface involving transition between y_1 and y_5, the Maxwell stress T* provides the only value of a at which such a surface can be located if the solution is to be stable in an absolute sense. In the event that T* is independent of r, it then follows from (42) and (43) that there is at most one radial location at which $a = r^*$, and this location varies with the applied external shear stress T *(b)* or, equivalently, the twist *y/* in (3). This is the case for homogeneous, isotropic materials, as discussed in Abeyaratne

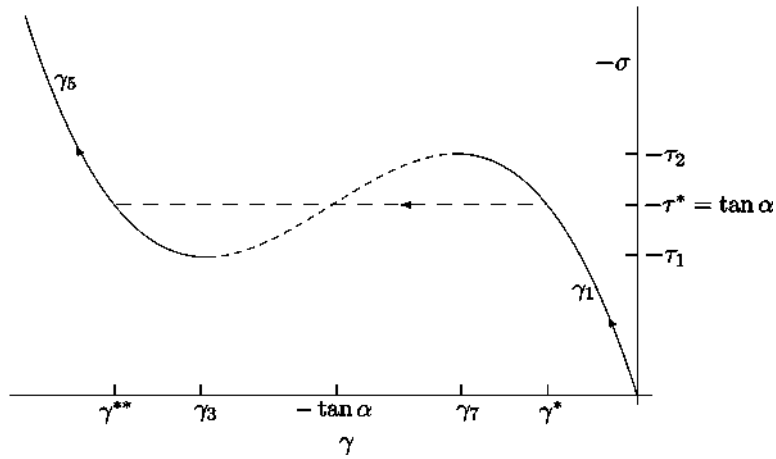

Figure 7. Representative plot of —*a(y),* as given by (43), against *y* (< 0). As —*a* increases from zero the continuous curve is followed until —*a* reaches the value —r* > —z\, at which point this path loses stability and the solution jumps to the left-hand continuous part of the curve, which is stable as — *a* increases further. The stable path is indicated by the arrows. The horizontal dashed line at *a* = *z** is the Maxwell line, for which the two closed regions cut off the curve have equal areas. The dashed part of the curve and the continuous parts for $y_7 < y_x < y^*$ and $y^{**} < y_5 < y_3$ correspond to unstable solutions.

and also for the materials considered here provided that all constitutive parameters (including *a)* are independent of r. More general possibilities apply if *a* depends on r.

The sense in which such solutions are absolutely stable , namely, for the same boundary conditions, such a solution minimizes the overall energy with respect to all other deformations, either smooth solutions or those containing one or more discontinuity surfaces. This eliminates consideration of the branch of solutions associated with any descending branch in Figure 2, i.e. y_4, and also eliminates y_1 *if* $y_7 < y_1 < y^*$ and y_5 if $y^{**} < y_5 < y_3$. It is worth observing here that such unstable y_1 and y_5 can be regarded as metastable in the sense that solutions involving these values are minimizers with respect to continuously differentiable variations in the twist function *g(r)* in (2). Since, however, such continuously differentiable variations permit neither the formation of new discontinuity surfaces nor the alternative placement of existing discontinuity surfaces, they do not address the absolutely stable solutions that we consider here. Hence the condition for the stability of the shear strain y_1 (and instability of y_5) is

$$\tilde{W}(\gamma_5) - \tilde{W}(\gamma_1) - \sigma(\gamma_5 - \gamma_1) > 0, \tag{66}$$

where $\sigma = \sigma(\gamma_1) = \sigma(\gamma_5)$. In the context of isotropic elasticity the stability analysis has been discussed in detail by Abeyaratne and the present situation follows closely that analysis.

We remark here that Equation (65) is the specialization of the admissibility condition $[\![W\mathbf{I} - \mathbf{F}^{\mathrm{T}}\mathbf{S}^{\mathrm{T}}]\!]\mathbf{N} = \mathbf{0}$ for equilibrium shocks , where $[\![\ ]\!]$ indicates the jump in the enclosed quantity across the surface with unit normal **N** in the reference configuration, **I** is the identity

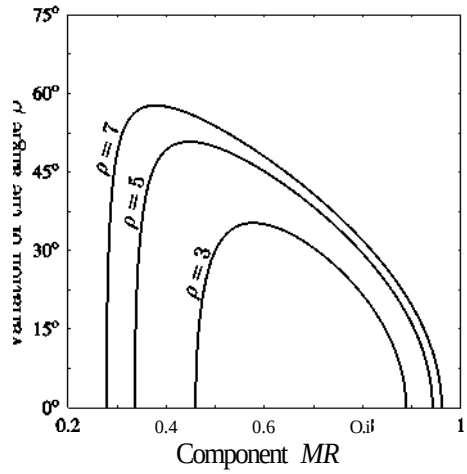

Figure 8. Plot of the angle /?*(> 0) against M_R for p =3,5,1.

tensor and S = F^{-1}c is the nominal stress tensor. This guarantees that quasi-static motion of an equilibrium shock (i.e. the surface of strain discontinuity) is dissipation-free.

It is easily shown from (43) that *a(—y* — 2 tana) + 2 tana = —*a{y),* which means that *a (y)* is antisymmetric about the point *y* = — tan *a, a* = — tan *a.* It follows that (65) provides the explicit Maxwell values *r** = — tana and

$$\gamma^{*} = -\tan\alpha + \frac{\sqrt{2\rho M_R^2 M_\Theta^2 - 1}}{\sqrt{2\rho}M_R^2}, \quad \gamma^{**} = -\tan\alpha - \frac{\sqrt{2\rho M_R^2 M_\Theta^2 - 1}}{\sqrt{2\rho}M_R^2}. \tag{67}$$

Note that *y* * is negative by virtue of (64).

Now, from $(2)_2$, (7)i, (9) and (10), we find that

$$r\frac{\mathrm{d}\theta}{\mathrm{d}r} = rG'(r) + rg'(r) = \tan\alpha + \gamma = \tan\beta, \tag{68}$$

where tan/? = *me/m*$_r$, i.e. /? is the angle (measured counterclockwise) between the deformed fiber direction and the radial direction e_r. Let /?* and /?** be the values of /? corresponding to the values *y* * and *y* ** in (67). It follows that tan/T > 0, tan/T* < 0 and *P*** + *p** = 0. This means that the deformed fiber directions on the two sides of the circle of discontinuity are symmetrically disposed relative to the e_r direction. Note that e_r is normal to the direction of shear. A similar symmetry arises in the rectilinear shear problem examined by Merodio . Note that /?* (and hence /?**) is non-monotonic as a function of M_R = cos a and has a maximum (minimum) at M_R = *l/«/p(p* > 2). Figure 8 shows the behavior of /?* as a function of M_R for three different values of *p* > *2.*

We close this section with a remark regarding the issue of selecting solutions since it is worth mentioning that other means for selecting solutions involving an elastostatic shock are also possible . Such alternative selection criteria have received a great deal of attention in the recent literature, especially as it relates to the continuum mechanical modeling of

solid-solid phase transformations. In these alternative resolutions, it is necessary to ensure that the selection criterion is consistent with the second law of thermodynamics . Furthermore, unlike the absolutely stable solutions considered here, such alternative resolutions would typically provide some hysteresis in the solution dependence on γ.

7. THE REINFORCED VARGA MODEL

An alternative representation for the strain-energy function is examined at this point. Instead of I_1, we use the principal invariant i_1 (= tr**V**) of the stretch tensor $\mathbf{V} = \mathbf{B}^{1/2}$. Analogously to (33), we consider the class of strain-energy functions

$$\check{W}(i_1, I_4) = \check{E}(i_1) + F(I_4), \tag{69}$$

and we note the connection $I_1 = i_1^2 - 2i_1$. Then,

$$\hat{W}(I_1, I_4) = \tilde{W}(\gamma, \alpha) = \check{W}(i_1, I_4), \quad E(I_1) = \check{E}(i_1). \tag{70}$$

For the problem under examination, we then have, on use of $(11)_1$,

$$i_1 = 1 + \sqrt{4 + \gamma^2}. \tag{71}$$

As a particular example, we now focus on the so-called Varga model, defined by

$$\check{E}(i_1) = 2\mu(i_1 - 3) = 2\mu\sqrt{4 + \gamma^2} - 2 = \tilde{E}(\gamma), \tag{72}$$

augmented by the same reinforcement $(38)_2$ in order to characterize the response of a transversely isotropic circular cylindrical tube under the pure azimuthal shear deformation. As for the neo-Hookean model, the parameter μ involved in (72) is the shear modulus of the isotropic base material, and the counterpart of (37) is

$$\check{W}(i_1, I_4) = \frac{1}{2}\mu\left[4(i_1 - 3) + \rho(I_4 - 1)^2\right]. \tag{73}$$

Since $\tilde{E}'(\gamma) = 2\mu\gamma/\sqrt{1 + \gamma^2}$ the monotonic nature of the function $\sigma(\gamma)$ associated with the Varga base material is apparent. Note, however, that, in contrast to the neo-Hookean base material $\tilde{E}'$ tends to a finite value as $\gamma \to \infty$.

The azimuthal equation (25) now specializes to

$$\sigma(\gamma) \equiv 2\gamma(4 + \gamma^2)^{-1/2} + 2\rho M_R^2 \gamma(M_R^2\gamma^2 + 3M_R M_\Theta \gamma + 2M_\Theta^2) = \tau(r). \tag{74}$$

Note that the finite asymptote for $\sigma(\gamma)$ persists for either $\rho = 0$ or $M_R = 0$. More generally, however, $\sigma(\gamma) \to \pm\infty$ as $\gamma \to \pm\infty$. Unlike its counterpart (43), equation (74) does not admit explicit expressions for γ, so that necessary and sufficient conditions for the uniqueness of γ are not in general obtainable in closed form. However, for $\gamma > 0$ it is easy to

show that $\sigma(\gamma)$ is a monotonic increasing function, and hence γ is determined uniquely for $\tau > 0$. Possible loss of uniqueness is, as for the model (37), strictly associated with negative γ. When $\tau(r) < 0$ equation (74) may have multiple roots for γ (< 0) even for very small values of the parameter ρ. As expected, an increase in ρ results in a decrease in the value of τ for which loss of uniqueness is initiated. In other words, we see that the analogues of $\tau_1(r)$ and $|\tau_2(r)|$, denoted $\check{\tau}_1(r)$ and $|\check{\tau}_2(r)|$, respectively, are monotonically increasing with ρ, so that larger values of ρ result in an expansion of the region encompassing multiple choices for γ.

It is therefore clear that the general qualitative properties of the boundary $\check{\tau}_1(r)$ are very similar to those of $\tau_1(r)$. Let us quantify the maximal set of points for which multiplicity of γ occurs, analogously to (48), by the inequalities

$$\check{M}_1 < M_R < \check{M}_2, \tag{75}$$

where $\check{M}_1 = \check{M}_1(\rho)$ and $\check{M}_2 = \check{M}_2(\rho)$. Then, for any fixed $\rho \geq 2$ we obtain the nesting

$$\check{M}_1 < M_1 \leq M_2 < \check{M}_2, \tag{76}$$

which, for all relevant r, leads to

$$\tau_1(r) < \check{\tau}_1(r) < 0, \tag{77}$$

but the relative disposition of $\tau_2(r)$ and $\check{\tau}_2(r)$ is not immediately clear and depends on r.

In the limiting cases where $\mathbf{M}$ is either radial or circumferential uniqueness of γ is, as for the model (37), guaranteed. For $M_R = 0$, (74) may be solved to give

$$\gamma = 2\tau(4 - \tau^2)^{-1/2}, \tag{78}$$

γ and τ having the same sign, so there is clearly an upper bound on $|\tau|$ for which the considered deformation is admissible, a point observed previously for the purely isotropic Varga model (see, for example, the general discussion in [2], which includes results for the Varga material as a special case). For $M_\Theta = 0$, on the other hand, a closed-form solution of (74) is not obtainable.

The variations of the boundaries $\check{\tau}_1(r)$ and $\check{\tau}_2(r)$ with respect to the component M_R are illustrated in Figure 9 for three fixed values of ρ. Also shown are the plots of the Maxwell stress $\check{\tau}^*(r)$ against M_R.

The requirement for (73) to be strongly elliptic is

$$\rho M_R^2(3M_R^2\gamma^2 + 6M_R M_\Theta \gamma + 2M_\Theta^2)(4 + \gamma^2)^{3/2} + 4 > 0, \tag{79}$$

which is, as for its counterpart (62), automatically satisfied throughout the body for positive γ. For negative γ, on the other hand, violation of (79) may now occur for any $\rho > 0$, although the associated non-strongly-elliptic domain cannot be identified explicitly. Numerical calculations, however, show that the correlation between ellipticity failure and the existence of multiple values for γ is entirely analogous to that for the reinforced neo-Hookean model. Thus, the properties

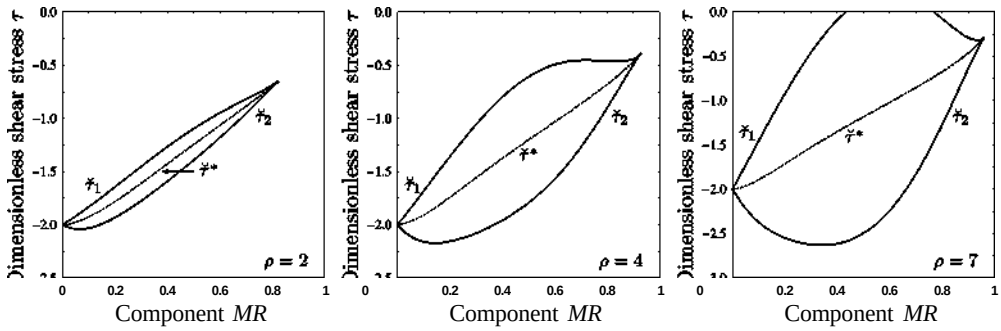

Figure 9. Plots of the limiting functions $\check{\tau}_1$ and $\check{\tau}_2$ against the component M_R for $\rho = 2, 4, 7$ for the reinforced Varga material. The dashed curves are plots of the Maxwell value $\check{\tau}^*$.

$$\check{\tau}_2(r) \leq \tau(r) \leq \check{\tau}_1(r) \tag{80}$$

associated with (75) serve to characterize the domain for which multiple values of γ arise and on the boundary of which ellipticity fails.

It is worth mentioning here that, as for (62), breakdown of (79) is also possible at the limiting values $\check{M}_1$ and $\check{M}_2$, although there is no associated discontinuity in γ. This again corresponds to the emergence of a weak discontinuity in γ, i.e. a discontinuity in $\mathrm{d}\gamma/\mathrm{d}r$, at the appropriate value of r. Finally, we note that the possibility that (74) yields negative, and therefore physically inadmissible, values of γ for positive $\tau(r)$ may also arise here. More specifically, for ρ greater than about 6 there exists a subinterval of (75) in which multiplicity of γ, in conjunction with loss of ellipticity, occurs. For this subinterval, which varies with ρ, the boundaries of the domain where positive shear stress results in negative γ are determined via equation (74) by resolving the latter in the limit $\tau \to 0^-$. In the case $\rho = 7$, illustrated in the right-hand plot in Figure 10, such a subinterval can be observed.

The ellipticity status of the material model (73) is illustrated in Figure 10 for three values of ρ. The notations $\check{\gamma}_2$, $\check{\gamma}_3$, $\check{\gamma}_6$, $\check{\gamma}_7$ and $\check{\gamma}_4^*$, $\check{\gamma}_5^*$ have been adopted in parallel with those used in Section 6.3. In particular, the counterparts of Figures 3(b) and 4(b) are plotted for $\rho = 2, 4, 7$ in order both to highlight the connection between the existence of multiple values for γ and the notion of strong ellipticity. Plots of the values of $\check{\gamma}^*$, $\check{\gamma}^{**}$ associated with the Maxwell stress $\check{\tau}^*$ are also shown.

8. NUMERICAL EXAMPLES AND DISCUSSION

In this section we illustrate some aspects of the response of the model (37) under the considered deformation. For numerical purposes we fix the radial dimensions at $a = A = 1$ (units) and $b = B = 6$ (units), while the parameters p and $r(b)$ are specified separately for each example. Our main aim is to highlight the influence of the anisotropy parameter p and the preferred direction M on the overall response of the body.

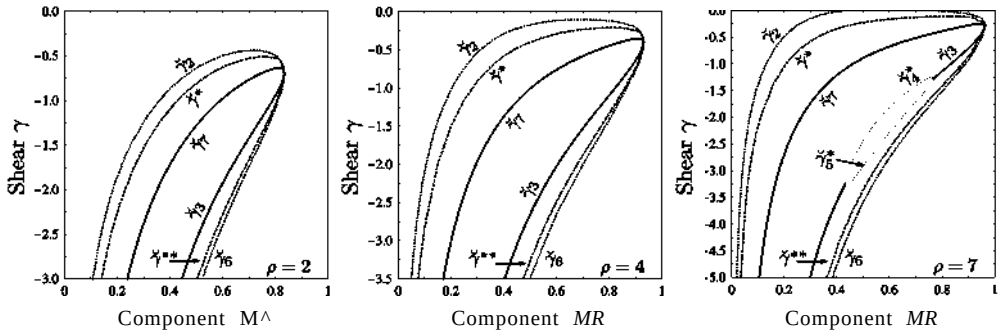

Figure 10. Characterization of the boundaries of the strongly elliptic domain (dotted curves) for the material model (73) in terms of the shear y (vertical axis) and M_R (horizontal axis) for p = 2,4, 7: the curves are given by y_2 and y_6. Also shown (continuous curves) are y_3 and y_7, within which the inequality (79) is reversed. The dotted loop in the right-hand plot is defined by the inadmissible values y^*_4 and f^*_5. Also shown for p = 2,4,7 are the (dashed) curves of the Maxwell values y^* and y'' corresponding to ?*.

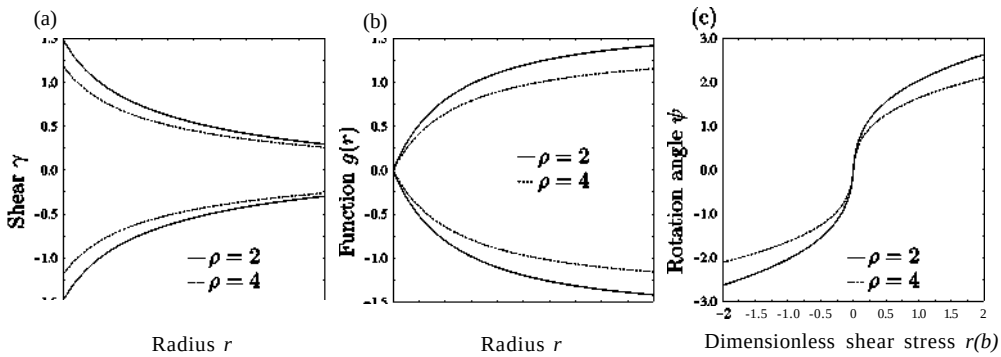

Figure 11. Plots of (a) the shear y, and (b) the function $g(r)$ against the radius r for the reinforced neo-Hookean model (37) with p = 2,4, M = E_R and $z(b)$ = ±0.4. In (c) the resulting rotation angle $yz = g(b)$ is plotted against $z(b)$ for p =2,4.

8.1. Radial Reinforcement

First, we examine the simple case in which M is radial. Then, bearing in mind that (37) is convex as a function of y in this case, the solution for y is unique and smooth. We observe that $|y|$ is a monotonic decreasing function of r, while, as expected, the corresponding solution $|g(r)|$ increases with r. Furthermore, for fixed $r(b)$, an increase in p results in a decrease in the value of $|y|$ and hence of $|g(r)|$ at any point of the body, whilst larger values of $r(b)$ yield larger strains. Clearly, because of the nature of the radial anisotropy considered here, the material response is the same for either sense of the shear. In Figure 11 we plot (a) the amount of shear y and (b) the associated rotation function $g(r)$ against the radius r for

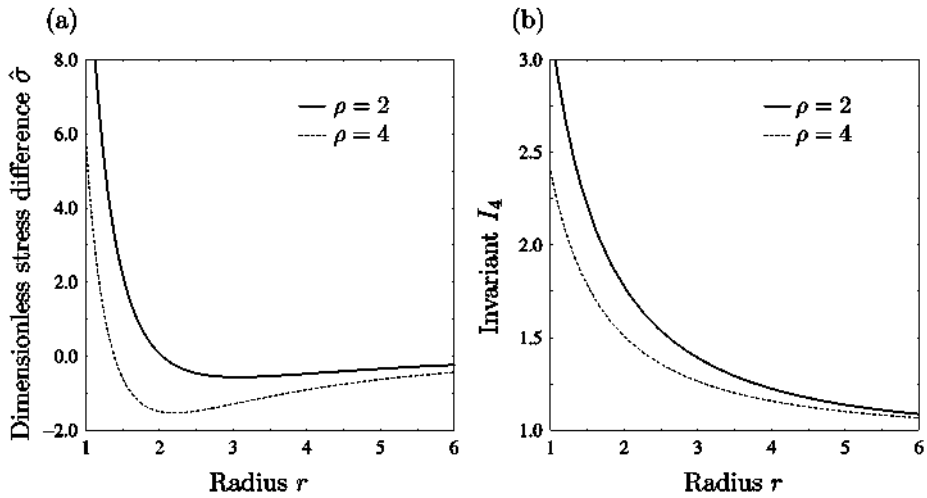

Figure 12. Plots of (a) the dimensionless stress difference *a,* and (b) the invariant 7_4 as functions of the radius *r* for the model (37) with *p = 2,*4, M = E_R and *z{b)* = 0.4.

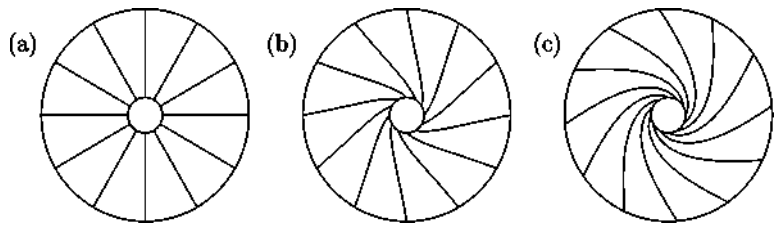

Figure 13. Cross-section of a tube undergoing positive (anticlockwise) pure azimuthal shear deformation: (a) the undeformed (stress-free) configuration with M = E_R; (b) *p =2, z(b)* = 0.2; (c) *p =2, z(b)* = 1.2.

*p = 2,*4 while in (c) the dependence of the rotation angle *y/* on *z (b)* is illustrated, again for *p = 2,*4. Both positive and negative shears are included so as to compare, in subsequent sections, with the unsymmetric situation between positive and negative shears when M is not radial.

In addition, for the same values of *z (b)* and *p,* the dimensionless stress difference *a = {dee — a_{rr})l'fi = r(da_{rr}/dr)/ju* and the invariant I_4 are plotted against r in Figure 12. We observe that both *a* and *h(>* 1) are larger on the inner boundary of the body. Unlike *y* , *a* and I_4 are invariant under change of sign of *zip).* In Figure 13 we demonstrate the results of the considered deformation on a cross section of a tube for a fixed value of the parameter *p* (= 2) and for two values of *z(b) (>* 0) so as to illustrate how the preferred direction changes under the deformation.

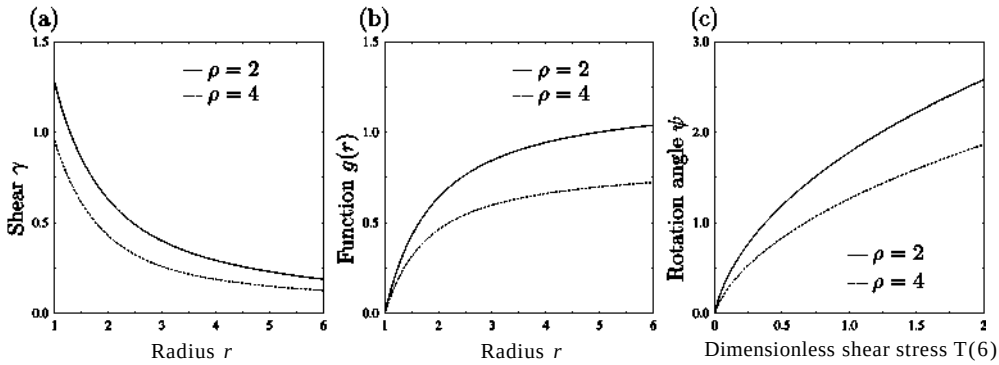

Figure 14. Plots of (a) the shear γ and (b) $g(r)$ versus the radius r for the model (37), with the anisotropy defined by the geometry (83): $\rho = 2, 4, \tau(b) = 0.4$. In (c) the rotation angle $\psi = g(b)$ is plotted as a function of $\tau(b)$ (> 0): $\rho = 2, 4$.

8.2. Reinforcement with Radially Varying α

For definiteness, we now consider the preferred direction to be defined by the family of curves

$$R = c_1(\Theta - \Theta_0) + c_2, \tag{81}$$

where $C\backslash$ and c_2 are constants. In respect of (81) the function *G(R),* according to the definition (7), takes the simple form

$$G(R) = (R - c_2)/c_1. \tag{82}$$

We choose 0o = 0 (radians) and, with reference to (7), 0i = 2 (rad), and then, for the specific values of *A* and *B* adopted here, we obtain $c\backslash = 2.5$ and $c_2 = 1$. Thus, from (82) the components (8) of M are given by

$$M_R = \frac{1}{\sqrt{(2R/5)^2 + 1}}, \quad M_\Theta = \frac{2R/5}{\sqrt{(2R/5)^2 + 1}}. \tag{83}$$

For this geometry, on application of positive shear, the overall response of the body is found to be similar to that for M = E_R. In fact, for r > 0, equation (43) guarantees smooth and unique values for *y.* Moreover, *y* and *g* are also monotonic functions of r, and changes in *r (b)* (> 0) and *p* have an analogous impact on the overall response of the body, as for the case of radial reinforcement. However, we remark that the dependence of M on r leads to stronger reinforcement of the material since the value of y_x is smaller at any r than for M = E_{fi} at the same shear stress and for the same value of *p.* It is also apparent that the values of *a* and *U* follow a similar pattern as functions of r. Results for the considered geometry are illustrated in Figure 14, in which the amount of shear and the function *g* are plotted against r for the same values of *r (b)* (> 0) and *p* as used in

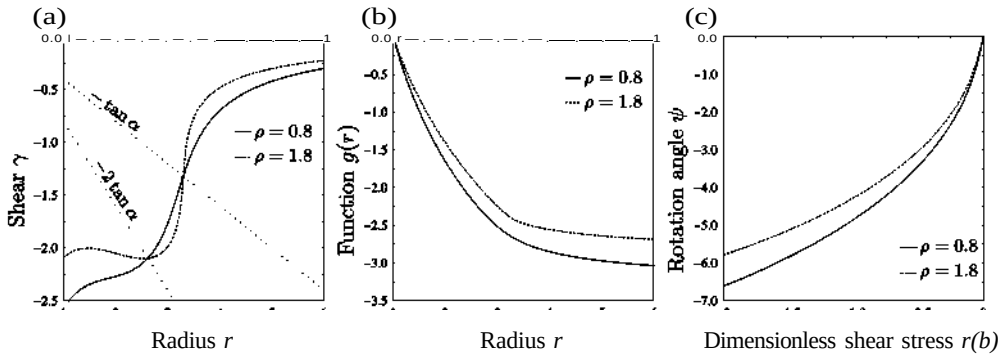

Figure 15. Plots of (a) the shear γ and (b) the function $g(r)$ versus the radius r for the model (37) with the anisotropy defined by the geometry (83): $\rho = 0.8, 1.8$, $\tau(b) = -0.4$. In (a) the (dotted) lines show the transitional values $-\tan\alpha$ and $-2\tan\alpha$, which depend linearly on r. In (c) the rotation angle $\psi = g(b)$ is plotted against $\tau(b)$ (< 0).

Figure 11. The dependence of the rotation angle ψ on $\tau(b)$ is also shown. The results should be compared with those in the upper halves of the plots in Figure 11.

The benign response of the material (37) with reinforcement (83) that was found to hold sway for positive shear does not always persist for negative shear. Specifically, as we now show, there is the possibility of loss of ellipticity, multiple values of γ and the emergence of discontinuity surfaces. For $\rho < 2$, the (unique, smooth) root γ_1 is now given by (44) with (83), but is not necessarily a monotonic function of r. In fact, monotonicity is only to be expected for sufficiently small values of $|\tau(b)|$ and for materials with a small value of ρ. Indeed, as ρ increases, loss of monotonicity of γ, associated with smaller magnitudes of the shear stress, is initiated closer to the inner boundary $r = a$ of the body, while an increase in $|\tau(b)|$ results in translation of such a point closer to $r = b$. Nevertheless, by writing $\gamma = \gamma(r)$ to indicate the dependence of γ on r, the property $|\gamma(a)| > |\gamma(b)|$ always holds. We emphasize, on the other hand, that the possible non-monotonic nature of γ is not reflected in that of g, which is monotonic in r, while variation of the parameter $\tau(b)$ does not modify these conclusions.

By contrast, the parameter ρ has a very crucial role. For a fixed value of $\tau(b)$, an increase in ρ leads to a decrease in the value of $|\gamma|$, but only for points for which $\tau(r) > -\tan\alpha$. If there is a point for which $\tau(r) = -\tan\alpha$ then γ would also take the value $-\tan\alpha$ there independently of the value of ρ (< 2), while, for points for which $-2\tan\alpha < \tau(r) < -\tan\alpha$, larger values of ρ correspond to smaller $|\gamma|$ until $\tau(r)$ reaches the value $-2\tan\alpha$, at which point we have $\gamma = -2\tan\alpha$, again independently of the value of ρ. For $\tau(r) < -2\tan\alpha$, the initial correlation between ρ and γ is recovered for all relevant r. Note that the above analysis applies for any $\mathbf{M}$ that depends on r. The consequences of negative shearing on a material incorporating the properties (37) and (83) are illustrated in Figure 15, in which the curves γ_1 and g are plotted as functions of r for a fixed value $\tau(b)$ (< 0) and for two values of ρ (< 2). Also plotted, in Figure 15(c), are the corresponding results for the rotation angle ψ as a function of $\tau(b)$. These plots should be contrasted with those in the lower halves of the plots in Figure 11.

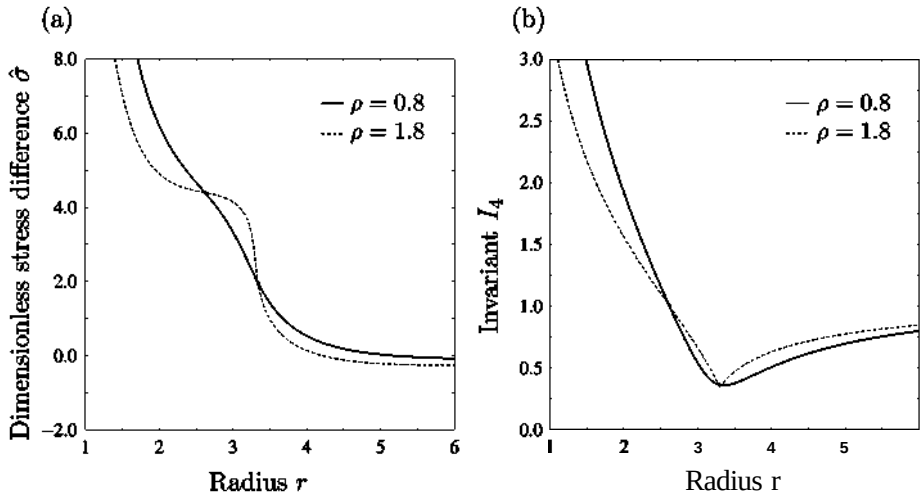

Figure 16. Plots of (a) the dimensionless stress difference $\hat{\sigma}$, and (b) the invariant I_4 against the radius r for the model (37) with (83) for $\tau(b) = -0.4$ and $\rho = 0.8, 1.8$.

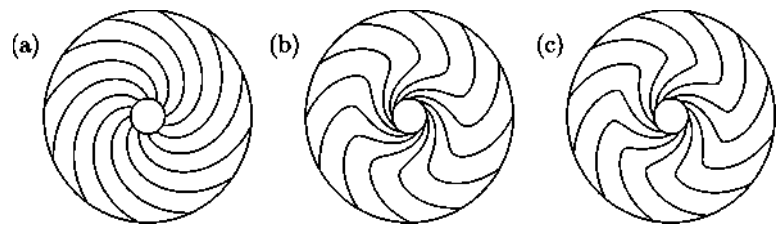

Figure 17. Cross-section of a tube undergoing a negative (clockwise) pure azimuthal shear deformation for the model (37) with the preferred direction defined by (83): (a) undeformed (stress-free) configuration; (b) deformed configuration with $\rho = 0.8$ and $\tau(b) = -0.4$ and (c) $\rho = 1.8$ and $\tau(b) = -0.4$.

In Figure 16, analogously to Figure 12, $\hat{\sigma}$ and I_4, are plotted against r for the same values of $\tau(b)$ and ρ used above to illustrate the variation of γ_1, while Figure 17 shows the effect of the deformation on the preferred direction for a tube cross-section with material characterized by (37) with (83). These plots should be contrasted with those in Figures 12 and 13, respectively. Although, on the scale shown here, there appears to be an abrupt change in the gradient of the deformed preferred direction in Figure 17(c) and an associated abrupt change in the corresponding curve for I_4 for $\rho = 1.8$ in Figure 16(b), in fact, since $\rho < 2$, the deformation is still smooth (there is no discontinuity in γ). As we show next, however, this smoothness is lost for $\rho > 2$.

Attention is now turned to the case where $\rho \geq 2$, for which, as explained previously in Section 6, negative shear may be associated with failure of strong ellipticity. For $\rho = 2$, the formulas (83) indicate that loss of ellipticity is confined to the surface $r = 2.5$ and only for

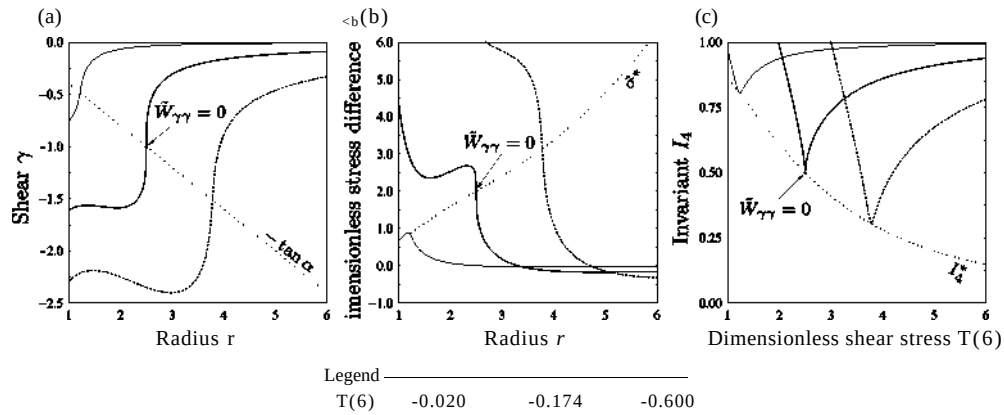

Figure 18. Plots of (a) the shear γ, (b) the dimensionless stress difference $\hat{\sigma}$, and (c) the invariant I_4 versus radius r for the model (37) with (83), for $\rho = 2$ and, in each case, $\tau(b) = -0.02, -0.174, -0.6$. Only $\tau(b) = -0.174$ is associated with loss of ellipticity. In (a) the point of loss of ellipticity on the dotted line $-\tan\alpha$ is shown; the corresponding point in (b) and (c) is shown on the dotted curves indicated by $\hat{\sigma}^*$ and I_4^*, respectively.

the value $\tau(b) = -(2.5/6)^2 \approx -0.174$. For $\tau(b)$ both less than or greater than this value the deformation is everywhere elliptic. We recall that for $\rho = 2$ uniqueness and continuity of the shear strain $\gamma = \gamma_1$, as given by (44), holds for all r. The value $\tau(b) = -0.174$ gives the temporary appearance of a cusp in the plot of I_4 at $r = 2.5$. These effects are shown in Figure 18. It should also be noted that high slopes in the γ_1 and $\hat{\sigma}$ curves are to be expected for points where $\gamma = -\tan\alpha$, or, equivalently, $\tau(r) = -\tan\alpha$, while for the same points the curves of I_4 exhibit rapid change. However, a true kink obtains only for the specific value $\tau(b) = -0.174$, at which ellipticity is temporarily lost.

As ρ increases, the domain $M_1 \leq M_R \leq M_2$ expands and therefore strong ellipticity can fail both for a wider range of loading values $\tau(b)$ and a wider range of locations r. This is exhibited in Figure 19, which shows how the region of non-strong-ellipticity, which is quite narrow, expands with ρ in a plot of $|\tau(b)|$ against r. The previously discussed case of $\rho = 2$ gives the single point $(r, \tau(b)) = (2.5, -0.174)$, whereas the $\rho > 2$ regions are nested within each other. This is not apparent from the figure since in order to distinguish the curves they are shifted vertically by different amounts. At $\rho = 3.9668$ the nonelliptic region first encounters one of the external boundaries, namely $r = 6$, while the boundary $r = 1$ is reached for $\rho = 4.205$. For $\rho > 4.205$ strong ellipticity can fail at any point of the body.

We now focus attention on the case $\rho = 3$ for which we note, as reflected in Figure 19, that failure of ellipticity is associated with the radial values

$$1.294 \lesssim r \lesssim 4.829, \tag{84}$$

and the associated range of loadings

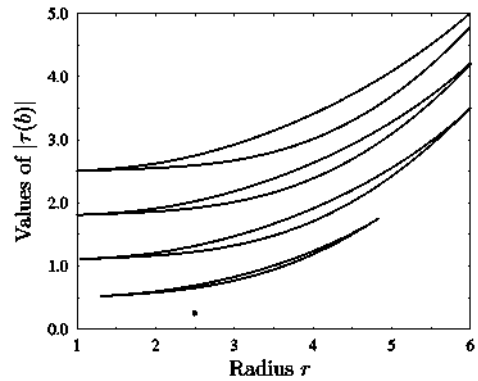

Figure 19. Plots of the values of $|\tau(b)|$ corresponding to loss of ellipticity against the radius $r \in [1, 6]$ for $\rho = 2, 3, 3.9668, 4.205, 5$. For $\rho = 2$ there is an isolated point at $r = 2.5$, $\tau(b) = -0.174$; $\rho = 3.9968$ corresponds to the value at which the curve just reaches the boundary $r = 6$; similarly for $\rho = 4.205$ and the boundary $r = 1$. The plots are nested, with each successive curve (for increasing ρ) enclosing the previous one, but have been shifted vertically, by $0.1, 0.5, 1.1, 1.8, 2.5$, respectively, to enable them to be distinguished.

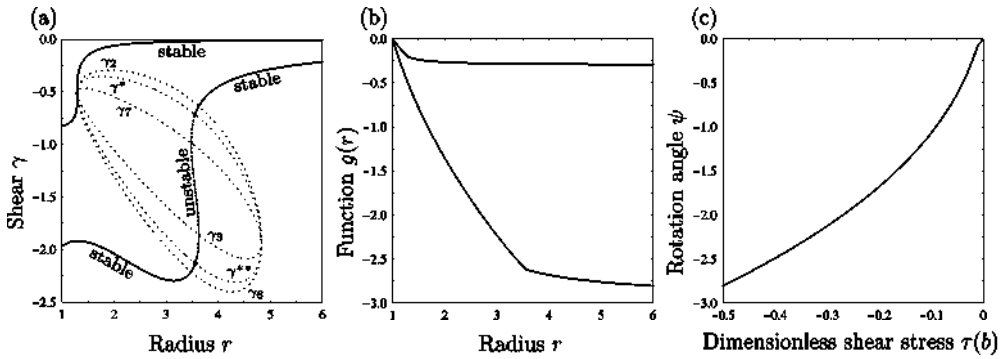

Figure 20. Plots of (a) the shear γ and (b) the function $g(r)$ versus the radius r for the model (37) with anisotropy defined by the geometry (83): $\rho = 3$ and $\tau(b) = -0.0241, -0.5$. In (c) the rotation angle $\psi = g(b)$ is plotted against $\tau(b)$ (< 0). The dotted curves in (a) are plots of $\gamma_2, \gamma_3, \gamma_6, \gamma_7, \gamma^*, \gamma^{**}$, as indicated.

$$0.0241 \lesssim |\tau(b)| \lesssim 1.2517. \tag{85}$$

As shown in Figure 20(a), in which γ is plotted as a function of r, loss of convexity of the strain energy (37) at $r \approx 1.294$, requiring $|\tau(b)| \approx 0.0241$, does not yield a discontinuity in γ. On the other hand, for any $\tau(b)$ such that $0.0241 < |\tau(b)| < 1.2517$ the inequality $\tilde{W}_{\gamma\gamma} \leq 0$ always holds within a subinterval of $1.294 < r < 4.829$, leading to multiple values for γ. In each case, however, it is possible to construct a unique non-smooth stable solution through the body by placing an elastostatic shock at the location where σ matches the Maxwell value τ^*. Figure 20(b) shows the consequence of the non-smooth solution on

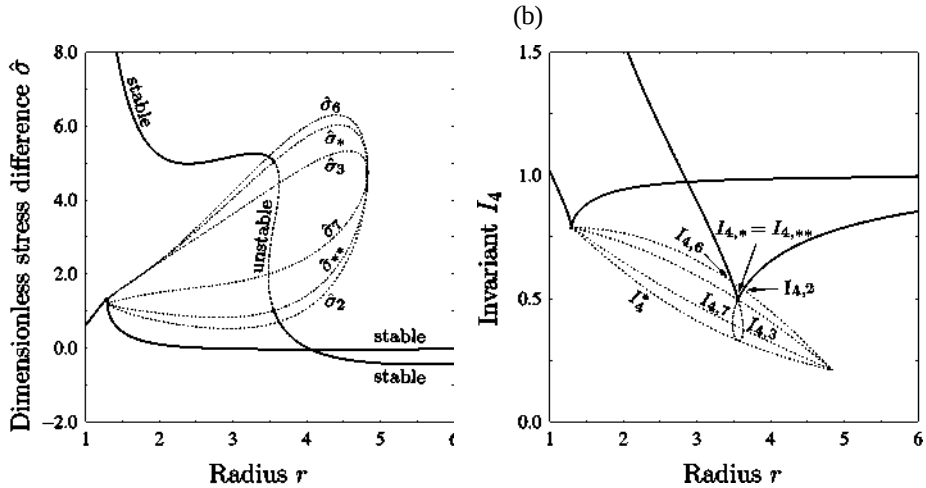

Figure 21. Plots of (a) the dimensionless stress difference $\hat{\sigma}$, and (b) the invariant I_4 in terms of the radius r for the model (37) with (83) and $\rho = 3$ for $\tau(b) = -0.0241, -0.5$. In (a) the symbols $\hat{\sigma}_2, \hat{\sigma}_3, \hat{\sigma}_6, \hat{\sigma}_7, \hat{\sigma}_*, \hat{\sigma}_{**}$ identify the values of $\hat{\sigma}$ associated with $\gamma_2, \gamma_3, \gamma_6, \gamma_7, \gamma^*, \gamma^{**}$; in (b) the corresponding values of I_4 are labelled $I_{4,2}$, $I_{4,3}$, $I_{4,6}$, $I_{4,7}$, $I_{4,*}$, $I_{4,**}$.

the curve $g(r)$ (discontinuity in the tangent), while the rotation (twist) angle ψ is plotted as a function of $\tau(b)$ in Figure 20(c). On close inspection a kink in the latter curve at $\tau(b) = -0.0241$ can be discerned.

Clearly, since both $\hat{\sigma}$ and I_4 depend on γ, any discontinuity in γ is reflected in the curves $\hat{\sigma}$ and I_4 that are plotted in Figures 21(a) and (b), respectively. In (a) the notations $\hat{\sigma}_2, \hat{\sigma}_3, \hat{\sigma}_6, \hat{\sigma}_7, \hat{\sigma}_*, \hat{\sigma}_{**}$ serve to identify the values of $\hat{\sigma}$ associated with $\gamma_2, \gamma_3, \gamma_6, \gamma_7, \gamma^*$, γ^{**}, respectively. Similarly, the symbols $I_{4,2}$, $I_{4,3}$, $I_{4,6}$, $I_{4,7}$, $I_{4,*}$, $I_{4,**}$ identify the corresponding values of I_4 in (b). Note, however, that a jump in $\hat{\sigma}$ is due to that in $\sigma_{\theta\theta}$ since σ_{rr} is continuous.

For the following discussion we use the notation τ_f and τ_s, respectively, for the values $\tau(b) = -0.0241$ and $\tau(b) = -1.2517$, the subscripts indicating "first" and "second". It follows that absolutely stable solutions contain an equilibrium shock for $\tau_s < \tau < \tau_f < 0$. Imagine therefore that the originally undeformed cylinder is subject to decreasing (dimensionless) shear stress $\tau(b)$ and consider the associated quasi-static progression of absolutely stable solutions. The associated deformations are continuous and smooth until $\tau(b) = \tau_f$ at which point loss of ellipticity takes place at $r = 1.294$. Further decrease in $\tau(b)$ gives rise to an elastostatic shock, initially at $r = 1.294$, which separates the two different elliptic values $\gamma = \gamma_1$ and $\gamma = \gamma_5$. Under continued decrease in $\tau(b)$, this discontinuity surface increases its radial location, before eventually disappearing at $r = 4.829$ when $\tau(b) = \tau_s$. For $\tau(b) < \tau_s$ the deformation is again classically smooth. The connection between the radial location r of the elastostatic shock and $\tau(b)$ is given simply by the formula $\tau(r) = \tau^* = -\tan\alpha$, which, since $\tau(r) = \tau(b)b^2/r^2$ and $\tan\alpha = 2r/5$, yields $r^3 = -90\tau(b)$. The discontinuity is highlighted in Figure 22, which shows the deformed cross-section of the tube for two values of $\tau(b)$ compared with the reference configuration.

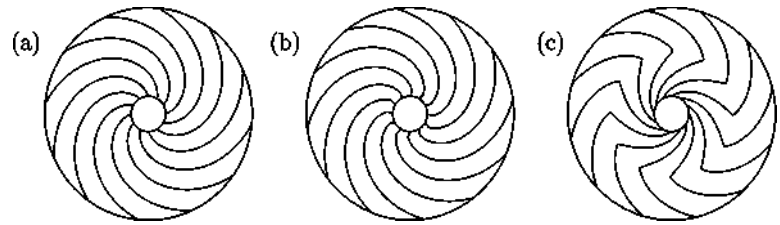

Figure 22. Cross-section of a tube undergoing negative (clockwise) pure azimuthal shear deformation for the model (37) with the preferred direction defined by (83): (a) undeformed (stress-free) configuration; deformed configuration with (b) $\rho = 3$ and $\tau(b) = -0.0241$ and (c) $\rho = 3$ and $\tau(b) = -0.5$.

The first, $\tau(b) = -0.0241$, heralds the emergence of the shock, whereas the shock has both increased its strength and its radial location at the second value $\tau(b) = -0.5$. Note that the associated kink in the case $\tau(b) = -0.0241$ (Figure 22(b)) is close to the inner boundary and is hardly noticeable in the figure. Across the shock the angles made by the two deformed preferred directions are symmetrically disposed with respect to the local radial direction in accordance with the discussion in Section 6.3. We recall that Figure 8 shows the kink angle β^* as a function of M_R, including the case $\rho = 3$ considered here. Since, for the considered geometry, $\tan\alpha = 0.4r$ we have $M_R = 1/\sqrt{1 + 0.16r^2}$, from which the behavior of β^* as a function of r can be deduced. The preferred direction is found to be maximally kinked at $r \approx 3.536$, corresponding to $\tau(b) \approx -0.491$.

It is worth emphasizing that by taking $\alpha = \alpha(r)$ the tube has been rendered effectively inhomogeneous. This has permitted the quasi-static shock discussed above in connection with Figure 21 to remain confined within the tube interior regardless of the magnitude of the twist ψ (equivalently of $\tau(b)$). This contrasts with the situation described by Abeyaratne [6] in which the shock always emerges at the inner radius and travels all the way to the outer radius as the twist magnitude increases. From a practical perspective, such internally confined shocks could present challenges for the assessment of any damage associated with shock formation and movement.

Broadly similar results to those described above for the reinforced neo-Hookean model (37) have been obtained for the material model (73) and we do not report them separately. Generally, the Varga model represents a material whose energy absorption capacity is low, and even for very small values of ρ a negative shear deformation yields almost immediate ellipticity breakdown.

Acknowledgments. The work of F. Kassianidis is supported by the U.K. Engineering and Physical Sciences Research Council and by the University of Glasgow. That of T. J. Pence was supported by a Visiting Fellowship grant from the U.K. Engineering and Physical Sciences Research Council.

REFERENCES

Rivlin, R. S. Large elastic deformations of isotropic materials VI. Further results in the theory of torsion, shear and flexure. *Philosophical Transactions of the Royal Society of London A*, 242, 173–195 (1949).

Jiang, X. and Ogden, R. W. On azimuthal shear of a circular cylindrical tube of compressible elastic material. *Quarterly Journal of Mechanics and Applied Mathematics*, 51, 143–158 (1998).

Jiang, Q. and Beatty, M. F. On compressible materials capable of sustaining axisymmetric shear deformations. Part 4. Helical shear of anisotropic hyperelastic materials. *Journal of Elasticity*, 62, 47-83 (2001).

Tsai, H. and Fan, X. Anti-plane shear deformations in compressible transversely isotropic materials. *Journal of Elasticity*, 54, 73-88 (1999).

Merodio, J., Saccomandi, G. and Sgura, I. The rectilinear shear of fiber-reinforced incompressible non-linearly elastic solids. *International Journal of Non-Linear Mechanics*, 42, 342-354 (2007).

Abeyaratne, R. C. Discontinuous deformation gradients in the finite twisting of an incompressible elastic tube. *Journal of Elasticity*, 11, 43-80 (1981).

Triantafyllidis, N. and Abeyarante, R. C. Instability of a finitely deformed fiber-reinforced elastic material. *Journal of Applied Mechanics*, 50, 149-156 (1983).

Qiu, G. Y. and Pence, T. J. Remarks on the behavior of simple directionally reinforced incompressible nonlinearly elastic solids. *Journal of Elasticity*, 49, 1-30 (1997).

Qiu, G. Y. and Pence, T. J. Loss of ellipticity in plane deformation of a simple directionally reinforced incompressible nonlinearly elastic solid. *Journal of Elasticity*, 49, 31-63 (1997).

Merodio, J. and Ogden, R. W. Material instabilities in fiber-reinforced nonlinearly elastic solids under plane deformation. *Archives of Mechanics*, 54, 525-552 (2002).

Merodio, J. and Ogden, R. W. Instabilities and loss of ellipticity in fiber-reinforced compressible non-linearly elastic solids under plane deformation. *International Journal of Solids and Structures*, 40, 4707-4727 (2003).

Abeyaratne, R. C. Discontinuous deformation gradients in plane finite elastostatics of incompressible materials. *Journal of Elasticity*, 10, 255-293 (1980).

Merodio and R. W. Ogden, Mechanical response of fiber-reinforced incompressible nonlinearly elastic solids. *International Journal of Non-Linear Mechanics*, 40, 213-227 (2005).

Merodio, J. and Pence, T. J. Kink surfaces in a directionally reinforced neo-Hookean material under plane deformation: I. mechanical equilibrium. *Journal of Elasticity*, 62, 119-144 (2001).

Merodio, J. and Pence, T. J. Kink surfaces in a directionally reinforced neo-Hookean material under plane deformation: II. Kink band stability and maximally dissipative band broadening. *Journal of Elasticity*, 62, 145-170 (2001).

Fu, Y B. and Zhang, Y. T. Continuum-mechanical modelling of kink-band formation in fibre-reinforced composites. *International Journal of Solids and Structures*, 43, 3306-3323 (2006).

Ericksen, J. L. Equilibrium of bars. *Journal of Elasticity*, 5, 191-201 (1975).

R. C. Abeyaratne, An admissibility condition for equilibrium shocks in finite elasticity. *Journal of Elasticity*, 13, 175-184(1983).

Abeyaratne, R. and Knowles, J. K. On the dissipative response due to discontinuous strains in bars of unstable elastic material. *International Journal of Solids and Structures*, 24, 1021-1044 (1988).

Knowles, J. K. On the dissipation associated with equilibrium shocks in finite elasticity. *Journal of Elasticity*, 9, 131-158 (1979).